UNIVERSITY OF SOUTHAMPTON

FACULTY OF ENGINEERING, SCIENCE AND MATHEMATICS

School of Engineering Sciences / School of Chemistry

Novel Aluminium Air Batteries for Ultralight Micro-Aircraft

by

Andrew D. Kay MPhys (Hons)

Thesis for the degree of Master of Philosophy

September 2005

UNIVERSITY OF SOUTHAMPTON

ABSTRACT

FACULTY OF ENGINEERING, SCIENCE & MATHEMATICS

SCHOOL OF MATERIALS ENGINEERING

Master of Philosophy

NOVEL ALUMINIUM AIR BATTERIES FOR ULTRALIGHT MICRO-AIRCRAFT

By Andrew David Kay MPhys (Hons)

This thesis investigates the feasibility of using a structural aluminium air battery to power an ultralight, unmanned micro-aircraft. Weight loss, voltammetry and scanning electron microscopy have been used to investigate the rate of corrosion and anodic dissolution of aluminium materials in potential battery electrolytes. Various alloys were examined in both alkaline and saline electrolytes and there were substantial differences in corrosion resistance, types of corrosion and overpotential required for anodic dissolution. It was found that high purity aluminium and alloys with small additions of certain metals had better corrosion resistance in alkaline solution. No materials investigated would allow extended storage of a battery; emphasis was therefore placed on a cell where 8M KOH was added immediately before discharge. AB50V, an Al-Mg-Ga-Sn alloy, was selected as the negative electrode in a small aluminium-air battery. This alloy had an open circuit potential of ~ -2.0 V vs. SCE and gave a current density of 100 mA cm^{-2} at ~ -1.8 V vs. SCE. A test battery cell was constructed incorporating a Pt-catalysed air cathode, and a battery voltage of ~1.3 V at a current density of 160 mA cm^{-2} was obtained using the AB50V alloy. The non-availability commercially of more alloys with fully specified compositions and a controlled range of compositions hampered both the scientific interpretation of the data and the optimisation of battery performance.

High surface area forms of aluminium should substantially improve this performance but are only available commercially in Al of unspecified composition. Commercially available Al foams were found to corrode very rapidly. Stacked meshes made with meltspun aluminium were compressed, and although they showed reasonable structural strength, did not show the required performance; meltspun fibres are inherently impure due to the fabrication process and so were unsuitable for making high purity alloys.

With the low weight of the current structural polymer foam used in production of the UAV, the positioning of the battery system on the plane is constrained to a skin around the nose cone. Such a design would, however, provide additional structural support to the aircraft, increase significantly the volume for electronics and sensory equipment in the pod, and reduce heating of such equipment by the battery operation.

List of Tables and Illustrations

Acknowledgements

I would like to thank both Professor Derek Pletcher and Professor Robert Wood for their support and help throughout the past two years. Thanks must also extend to Professor Richard Jones and Mr. Ian Wilcock from dstl for their funding and help.

My last thanks must go to my parents and my girlfriend for their unerring support throughout the project.

Glossary of Symbols

C_o / C_R	Concentration of reactant / mol m^{-3}
E	Potential vs. Reference electrode / V
E_e	Equilibrium potential / V
E_e^o	Formal electrode potential / V
F	Faraday Constant / F mol^{-1}
j	Current density / A m^{-2}
j_o	Exchange current density / A m^{-2}
k_s	Standard rate constant / m s^{-1}
n	Number of electrons in electrode reaction / dimensionless
R	Gas Constant / J K^{-1} mol^{-1}
T	Temperature / K
α_A	Anodic transfer coefficient / dimensionless
α_C	Cathodic transfer coefficient / dimensionless
η	Overpotential ($E-E_e$) / V

1. Introduction

1.1 Unmanned Air Vehicles (UAVs)

1.1.1 What is a UAV?

An Unmanned Air Vehicle (UAV) is a powered aerial craft that is sustained in flight by either a pre-programmed flight control (Drone) or by remote control (RPV: Remote Piloted Vehicle). They range in size from less than six inches in diameter (micro UAV) to large autonomous jets. The earliest UAV was designed during the 1st World War, and they were used to train antiaircraft gunners in the 2nd World War [1]. It is only in the past 25 years that they have been investigated extensively for military use, especially by the US Government. They are a relatively cheap, reusable tool that reduces the risk to military personnel during combat situations. Most of the initial UAVs were used solely for surveillance purposes but already many are being used for weaponry purposes, such as the RQ-1 Predator fitted with AGM-114 Hellfire air-to-ground missiles [2]. The use of UAVs is still primarily in the reconnaissance and scouting fields.

1.1.2 Mission Objectives

Military manoeuvres are becoming increasingly dependent on remote-controlled reconnaissance vehicles. The principal focus for this research is to look into the feasibility of producing an unmanned air vehicle for surveillance purposes that is both small and light. It will be powered by an aluminium-air battery that forms an integral part of the aircraft structure yet can be quickly replaced. The UAV is designed to be carried by infantry into battle situations and either hand, or catapult, launched from the ground [3]. The craft payload will be sensory equipment but it remains almost certain that the mass budget for the power system will easily dwarf the payload budget. The current proposal is for a plane that is both autonomous and actively controlled and ideally a flight time approaching one hour is required – with current battery systems allowing ~ 20 minutes maximum flight time. The battery system is being designed for use with a specific UAV produced by Blue Bear Systems Research Ltd [4] – with exact specifications below. It is hoped that current research may lead to powering micro-vehicles on scales of less than a few inches [5].

Figure 1.2 shows a typical mission power profile for a surveillance mission using Blue Bear UAV.

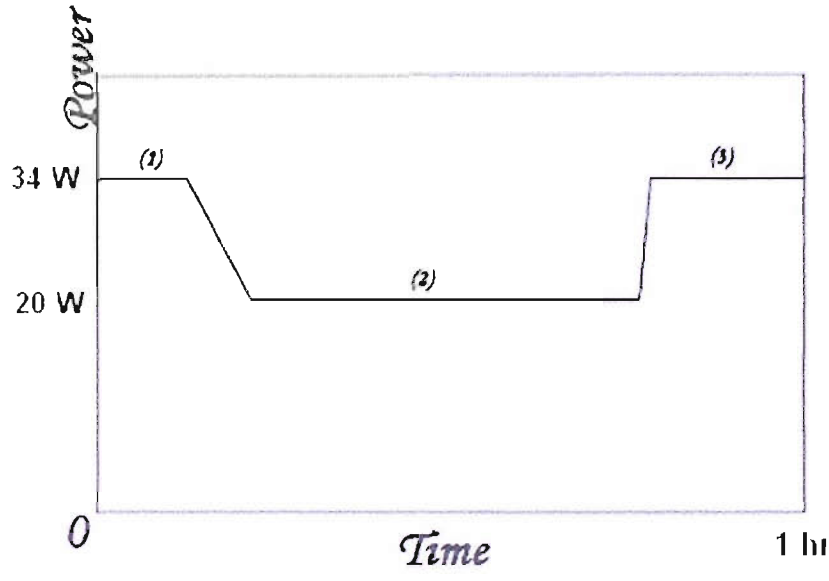

Figure 1.1 – An estimated Power/Time graph for a one hour typical flight.
(1) Launch and climbing to altitude, (2) cruise/straight flight, (3) Circling/Sensory equipment use.

The 34 W could be achieved with one 1.5 V cell delivering a current of ~ 20 A or, more likely, n x 1.5 V cells in series each delivering ~ $20/n$ A.

1.1.3 Blue Bear UAV Characteristics

Below is a table outlining the current performance of the prototype UAV that the battery system is being designed for [3]. *Figure 1.3* shows a photo of the current structure of the plane. It should be noted that the batteries are highly optimised, state-of-the-art Lithium polymer cells and that there is little possibility for significant improvement in performance. With the need for a fourfold improvement in power, new energy sources must be investigated.

Power System Information	
Voltage	7.4 V
Current Drawn	4.6 A (100% throttle) 2.8 A (60% throttle) 1.8 A (50% throttle) 1.2 A (40% throttle)
Charge	860 mA h
Battery Type	Lithium Polymer (Thunderpower [6])
Weight of Battery System	46 g
Structural Information	
Weight of Aircraft (including power and control systems)	200 g
Airframe Material	EPP Foam
Density of EPP Foam	35.2 kg m^{-3}
Mission Information	
Max. Flight Time	~ 23 minutes
Launch System	Hand / Catapult

Table 1.2 – A table showing the current characteristics achievable with the Prototype Plane setup [3]

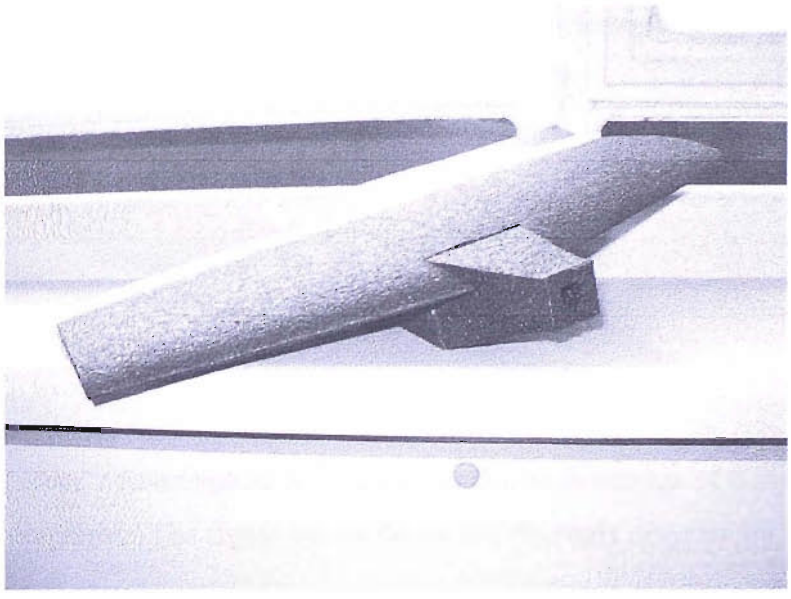

Figure 1.3 – A photo of the current shape of the Blue Bear Prototype plane (Taken 09/08/05)

1.2 Fundamentals of Electrochemistry

In general, the behaviour of electron transfer reactions e.g.

$$Al \rightarrow Al\ (III) + 3e^- \tag{1.1}$$

$$2H_2O + 2e^- \rightarrow H_2 + 2OH^- \tag{1.2}$$

are determined by both thermodynamics and kinetics.

Thermodynamics is usually discussed in terms of standard potentials that really concern the equilibrium:

$$2Al + 6\ H^+ \leftrightarrows 3H_2 + 2\ Al^{3+} \tag{1.3}$$

in 1M acid because they are quoted versus the standard hydrogen electrode.

A corrosion reaction can be pictured as two simultaneous electrode reactions occurring on the surface of the aluminium at anodic and cathodic sites [7]:

$$2H^+ + 2e^- \rightarrow H_2 \quad (1.4)$$

$$Al - 3e^- \rightarrow Al^{3+} \quad (1.5)$$

1.2.1 Thermodynamics

It has become commonplace to discuss the thermodynamics of corrosion reactions using Pourbaix diagrams. The figure below shows the Pourbaix diagram for aluminium.

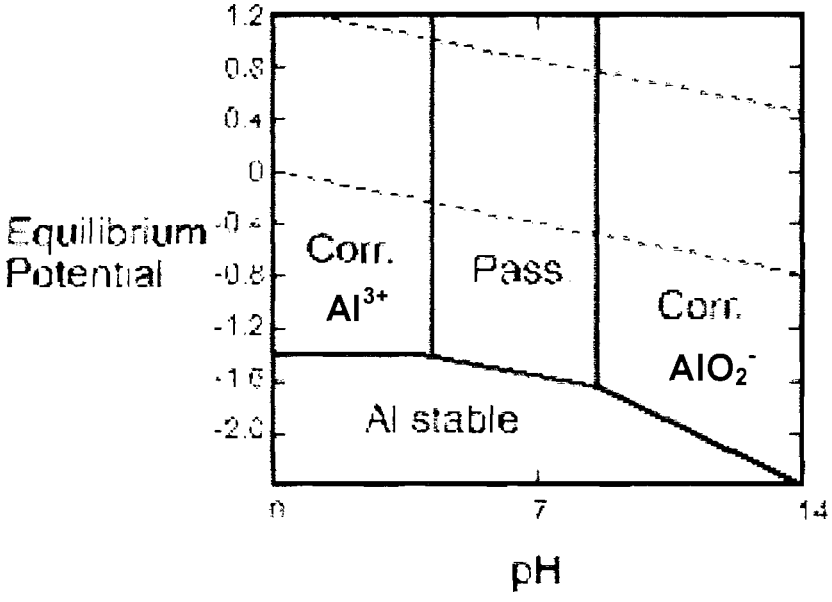

Figure 1.4 – Pourbaix diagram for Aluminium plotting equilibrium potential / V vs. pH [8].

The Pourbaix diagram above shows whether, at a certain potential and pH, pure aluminium has a tendency to corrosion, immunity, or forming a protective film. The two dashed lines show the equilibrium potentials for hydrogen evolution (lower line) and oxygen reduction (upper line). Because the Al / Al (III) line is always below the H^+ / H_2 and O_2 / H_2O lines, the diagram predicts that corrosion is always thermodynamically favourable. The diagram above shows four distinct regions that fall into three distinct groups:

(1) Al Stable – This is the immunity section where aluminium is thermodynamically immune to corrosion. It can only be achieved by applying a potential in the zone for stability.

(2) Corrosion - Here the tendency is for the aluminium to corrode producing either aluminium ions or soluble aluminium oxyanions.

(3) Passivation – This is a passive region where corrosion should occur but an oxide film is formed on the surface of the aluminium limiting further aluminium dissolution.

Although Pourbaix diagrams are a helpful tool they can only tell us what is possible not what will actually happen. It only considers the thermodynamical aspects of corrosion, ignores reaction rates, and can only be plotted for pure metals not alloys. They are also specific to the electrolyte solution considered.

1.2.2 Kinetics

Whilst the tendency for corrosion can be gauged by potential measurements and thermodynamic Pourbaix diagrams, it is not adequate to confidently state that the corrosion of aluminium will occur. The rate of the corrosion is a separate issue to the tendency to corrode, and so a high tendency may still be associated with a low rate of corrosion. The kinetics of electron transfer reactions are commonly discussed through the Tafel equation:

$$\log j = \log j_o + \frac{\alpha_A nF\eta}{2.3RT} \tag{1.6}$$

The two key features to examine in the above equation are j_o and η.

The exchange current density (j_o) is a measure of the equal levels of oxidation/reduction at the equilibrium potential.

$$j_o = nFk_s(C_o)^{\alpha_A}(C_R)^{\alpha_C} \tag{1.7}$$

Where k_s is the standard rate constant and is the rate constant for oxidation/reduction at the standard potential. Therefore, the exchange current density, and hence the rate of corrosion, depends on the standard rate constant and the concentration of each of the reactants. The equilibrium and standard potentials are related by the Nernst equation:

$$Ee = E_e^o + \frac{RT}{nF} \ln\left(\frac{C_o}{C_R}\right) \tag{1.8}$$

The overpotential (η) is defined as:

$$\eta = E - E_e \tag{1.9}$$

or the deviation of the potential from the equilibrium potential needed to cause current to flow. The overpotential is positive for anodic polarisation and negative for cathodic polarisation.

The corrosion potential is an example of a mixed potential. For example, the corrosion potential and corrosion current density for aluminium in potassium hydroxide depends on the thermodynamics and kinetics of both the Al / Al (III) and H_2O / H_2 couples.

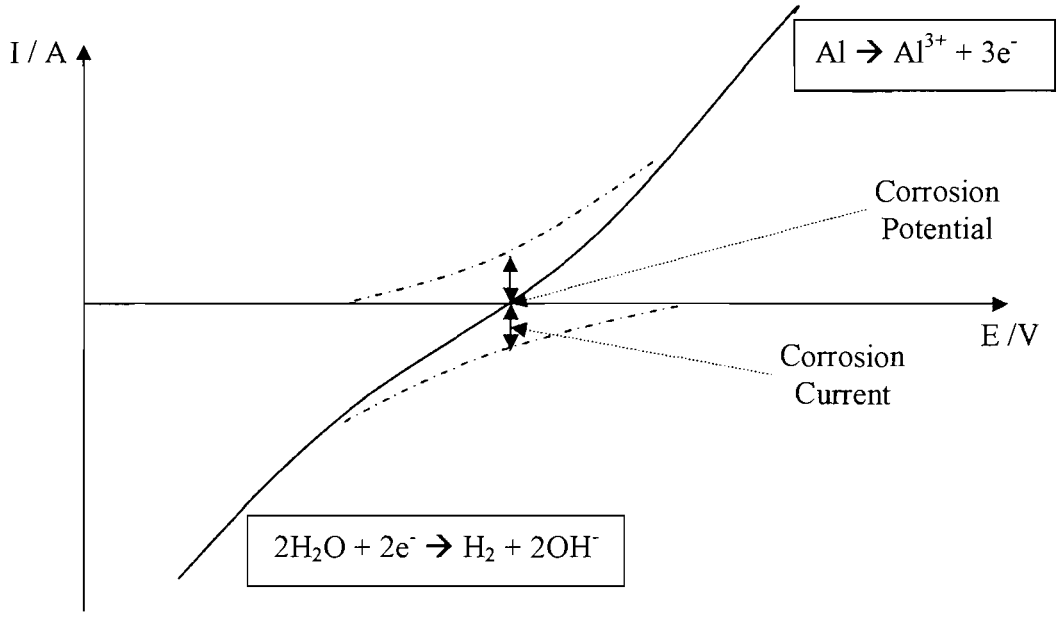

Figure 1.5 – Current-potential curves for Aluminium in deoxygenated, aqueous solution. The dotted curves show partial currents for aluminium dissolution and hydrogen evolution. Reproduced from [9].

The open circuit (corrosion) potential is where the current for oxidation of the aluminium equals that of the reduction of water (and/or oxygen). This current can be seen clearly on the voltammagram above. At the corrosion potential:

$$-I_{cathodic} = I_{anodic} = I_{corr} \tag{1.10}$$

I_{corr} can't be directly read from a voltammagram, but by converting the data into a steady state current for both aluminium oxidation and hydrogen evolution vs. potential it is possible to extrapolate to I_{corr}.

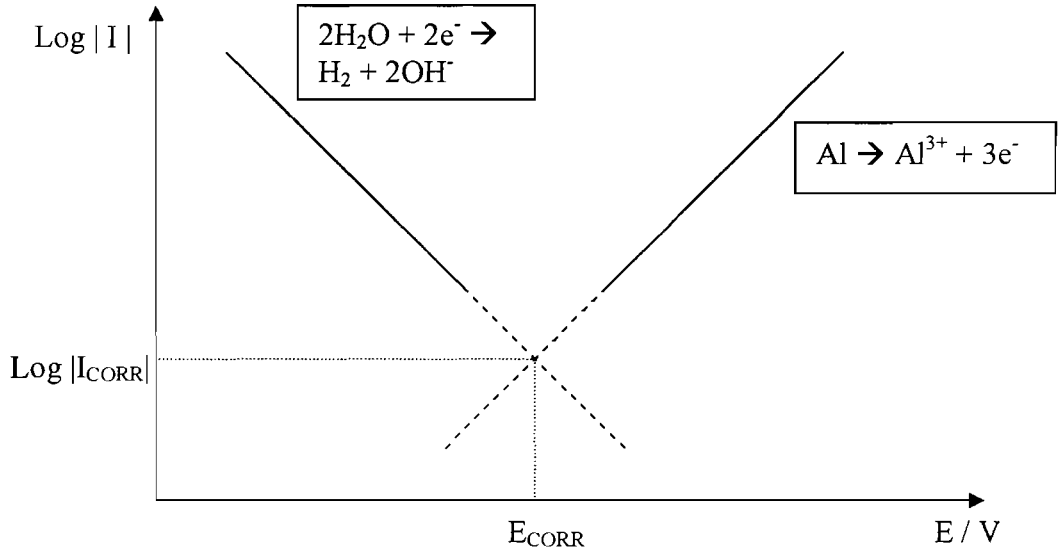

Figure 1.6 – A Log\|I\| vs. E /V plot for aluminium in deoxygenated, aqueous solution. The dashed lines show the extrapolation to find the corrosion potential (E_{CORR}) and the corrosion current (I_{CORR}). Reproduced from [9].

1.2.3 Passivation

Passivation is when a thin adherent film or layer is formed on the surface of the metal, creating a protective coating which limits further chemical reactions such as corrosion or electrochemical dissolution. In the case of aluminium, the passivating layer is that of aluminium oxide and occurs due to oxidation of the aluminium surface when in contact with aqueous solutions. If passivation occurs, a sudden drop in current is expected, which would then increase again when the overpotential was large enough.

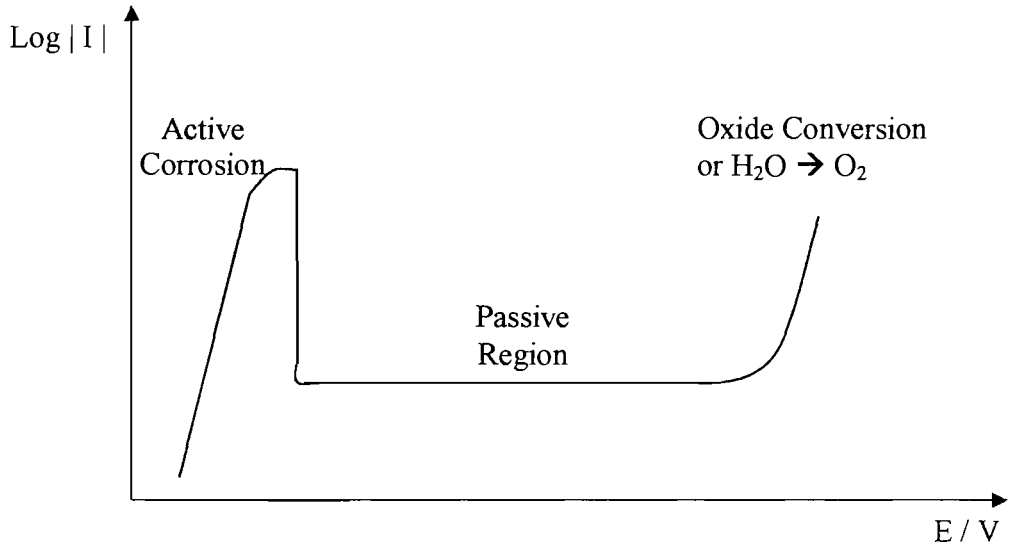

Figure 1.7 – A Log\|I\| vs. E/V plot for a metal showing passivation characteristics. Reproduced from [9].

The breakdown of the passive film leads to many of the common forms of corrosion failures, pitting, crevice, intergranular and stress. As well as electrochemical attack, mechanically rupturing the oxide film can lead to similar effects.

1.3 Aluminium

1.3.1 Aluminium-Air Batteries

Aluminium has been considered as a battery electrode since as long ago as the second half of the 19th century when Hulot [10] created a cell using aluminium as the cathode material. Its importance as an anode was first realised when it was used in the Buff Cell later that same century [11]. It was not until the early 1960s when real work began on the Aluminium-Air cell [12]; Zaromb and Trevethan et al. found that although the aluminium surface is covered by a passive oxide layer, it was possible to observe a higher voltage than in zinc-air systems [13].

Aluminium is a very attractive metal for use as a power source for a number of reasons. Its ability to transfer three electrons per atom, low atomic mass, a high theoretical energy density of 8.1 W h g^{-1}, and a high negative standard potential are all beneficial features. Combined with low production costs, structural benefits, and its large natural abundance, this makes aluminium extremely appealing for this purpose.

In the last decade the main focus of research and development has been on Al-Air systems using alkaline electrolyte, which allows for optimisation of the air cathode and low polarisation of the aluminium during normal operation. In an alkaline environment, the electrode reactions may be written [14]:

$$Al + 4OH^- \rightarrow Al(OH)_4^- + 3\,e^- \quad E_o \sim -2.35\ V \text{ vs. NHE} \tag{2.0}$$

And;

$$O_2 + 2H_2O + 4e^- \rightarrow 4\,OH^- \quad E_o \sim +0.40\ V \text{ vs. NHE} \tag{2.1}$$

for the negative and positive electrodes respectively.

Thus the overall reaction during discharge in alkaline solution is:

$$4Al + 3O_2 + 6H_2O + 4OH^- \rightarrow 4Al(OH)_4^- \quad , \quad E^\circ \sim 2.75V \text{ vs. NHE} \qquad (2.2)$$

Aluminium-Air batteries have never truly become a commercially viable battery - plagued by problems of corrosion of aluminium leading to minimal storage life, passivation, and difficulty in recharging/recycling – zinc-air systems have mostly been favoured. The main use for current Al-Air batteries are as primary reserve systems, where the electrolyte is added immediately prior to use, or as "mechanically" rechargeable batteries where the aluminium anode is replaced after each discharge.

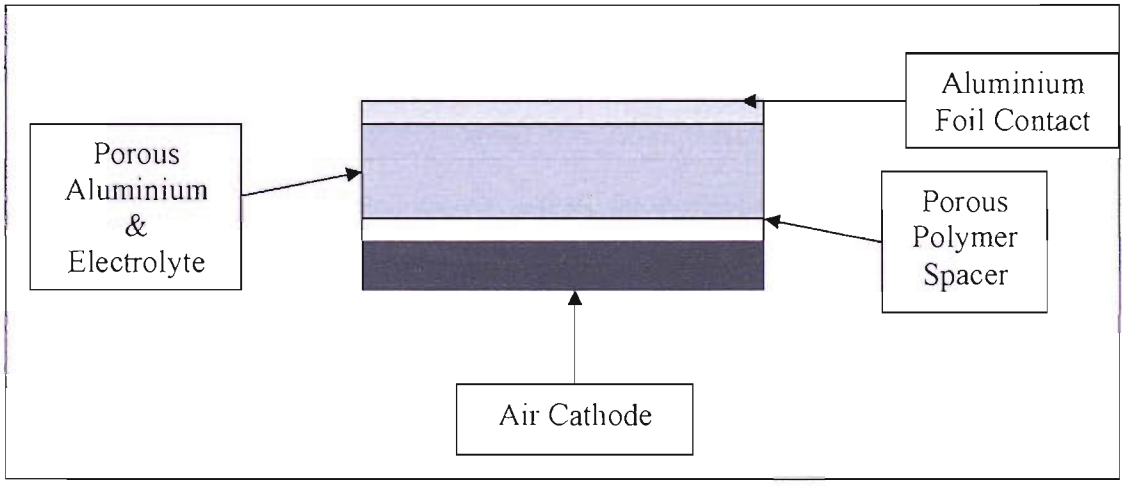

Figure 1.8 – Schematic of Aluminium-Air Battery Cell with a 3D aluminium anode. Not to scale.

In an Al-Air cell the aluminium anode is coupled to an air-breathing cathode which allows the passing of oxygen from the air outside whilst not allowing the electrolyte to leak out of the cell.

The actual voltage of the cell is inextricably linked to several variable factors. The overpotentials associated with the two electrode reactions, electrode gap, surface area of electrodes, current density drawn on discharge, alloy used, conductivity of electrolyte etc. are all key factors and will be covered later.

If we consider the expected estimated weight of each constituent part of the aluminium air battery:

Component	Weight / g	Note
Aluminium	0.6*	Using Faraday Law and Charge value from *Table 1.2.* Doubled to allow for structural integrity at end of discharge.
Air Cathode	0.06	Given a weight / surface area of 0.01 g cm^{-2}
Electrolyte	6[a]	Assuming 8M KOH with a solubility of alumina of ~ 8%

Table 1.9 – Estimated weight of aluminium air battery cell components in a typical cell allowing for one hours flight time at a current density draw of 30 $mAcm^{-2}$.

**** double the amount of aluminium needed to allow some structure to remain.***

[a] amount of electrolyte needed to stop precipitation assuming 8% solubility of alumina.

It is clear to see from the table above, that by far the largest mass consideration is that of the electrolyte. This means that either the solubility of the alumina in solution needs to be increased or some form of separation needs to occur.

1.3.2 The Air Cathode

Air cathodes are now highly developed components for fuel cells as well as cathodes in the chlor-alkali industry. In addition, for a number of years batteries with air cathodes have found many applications [15]. As a result, highly optimised air cathodes are commercially available from a number of sources.

The air cathode is usually a porous, electron-conducting, hydrophobic matrix – comprising a conducting mesh, e.g. carbon or nickel, as the current collector, pressed onto a carbon mat, impregnated with a platinum catalyst [16]. Many other catalysts have been investigated including Mn, Ag, Co and Ru, looking at both performance and cost [17].

Air cathodes are primarily optimised for use in alkaline environments, but if using saline solutions, then a nickel mesh is not advised. If left at open circuit conditions for a long period of time the potential of the active material in contact with the screen is high enough to oxidise the screen[18].

1.3.3 Other Metal/Air Batteries

In theory, several metal air batteries would be interesting to study:

Metal	Anode Reaction	Anode Potential *(vs. SHE)*	Metal Equiv. *Ah/g*	Cell Voltage *V*		Specific Energy Of Metal *(kWh/kg)*
				Theoretical	Operating	
Lithium	$Li + OH^- = LiOH + e^-$	-3.05	3.86	3.45	2.4	13.3
Aluminium	$Al + 3OH^- = Al(OH)_3 + 3e^-$	-2.35	2.98	2.70	1.2 – 1.6	8.1
Magnesium	$Mg + 2OH^- = Mg(OH)_3 + 2e^-$	-2.69	2.20	3.09	1.2 – 1.4	8
Calcium	$Ca + 2OH^- = Ca(OH)_2 + 2e^-$	-3.01	1.34	3.42	2.0	4.6
Iron	$Fe + 2OH^- = Fe(OH)_2 + 2e^-$	-0.88	0.96	1.28	1.0	1.2
Zinc	$Zn + 2OH^- = Zn(OH)_2 + 2e^-$	-1.25	0.82	1.65	1.0 – 1.2	1.3

Table 1.10 - A table showing the properties of current metal-air cells with alkaline electrolytes[14]

It is clear from Table 1.5 that aluminium is an extremely promising candidate for a metal-air battery. With the exception of lithium, aluminium shows the best specific energy and metal equivalent Ah / g. At present its operating cell voltage is considerably lower than theoretical values and the reasons for this will be discussed later. In practice, only zinc and aluminium have received serious consideration.

1.3.4 Present status of Aluminium-Air Batteries

Current uses for aluminium air batteries cover a considerable range of applications utilising the high energy density obtainable. The most common uses of aluminium air batteries are as reserve power supplies (with lead-acid batteries as the competition), used for back-up systems such as telecommunications equipment [19]. It is usually stored "dry" and then the electrolyte is added immediately prior to use and has such wide ranging uses

as mooring lights for barges, and field rechargers for nickel-cadmium and lead-acid batteries[14].

Aluminium has been heavily researched for use in powering electric vehicles [20-22]– containing about one-half the energy content of petrol per unit weight and three times the energy per unit volume [14]. It has also been under serious investigation by companies for use in mobile phones as a type of mechanically rechargeable battery [].
One of the most successful uses of aluminium-air batteries is in the underwater applications [23]. With sodium chloride being the electrolyte, the use of aluminium air batteries for underwater applications has several clear advantages; including long storage times when kept dry and a harmless electrolyte to aquatic life. It has been successfully used in applications from submarines to torpedoes [23].

There are a variety of novel designs for new aluminium-air setups, including the use of granular aluminium anodes [24] and even polymer/aluminium structures [25]. Unfortunately none of these are suitable for a light weight, shaped aluminium-air battery as considered for this application.

1.4. Aluminium as an Anode material

1.4.1 Aluminium as a power source

Although aluminium has many beneficial properties there are also several factors that have to be controlled in order for the battery system to be suitable for this application. Aluminium suffers from a parasitic corrosion reaction which results in coloumbic losses during discharge of the battery and a loss of fuel during standby. The latter can be rapid and negate any possibility of storage with electrolyte within the battery. It should also be noted that corrosion leads to hydrogen gas with the consequent safety hazards.

As well as the obvious dangers with the production of hydrogen, aluminium hydroxide is a gelatinous precipitate which can lead to clogging of the battery cell.

In saline and acidic media, the kinetics of the aluminium dissolution are governed by an oxide-hydroxide film covering the anode surface. In many industrial applications to inhibit atmospheric corrosion this film is pre-formed or altered to minimise the contact of the aluminium with oxygen and thus lower the corrosion of the aluminium [26-29]. Although the oxide film is successful in lowering the corrosion rate it also impedes the dissolution of the aluminium on discharge. In order to pit or remove this oxide film, it needs to be submerged in a strong alkaline solution or taken to a large positive overpotential in a solution where chloride ions are present. Indeed, the oxide formed in sulphuric acid is so passivating that structural aluminium components and window frames etc. are 'anodised' – a process where the aluminium is made the anode in an electrolytic cell.

The main electrolytes that have been studied include KOH, NaOH and NaCl [14, 16, 30-47], but many other electrolytes have undergone marginal research [48, 49], including ethanol [50], and even some non-aqueous electrolytes[45, 51].

1.4.2 Open Circuit Corrosion

One of the main problems that needs to be overcome to produce a fully-optimised Al-Air battery is the large open circuit corrosion rate that occurs in many system setups. Open circuit corrosion means that the useful storage life of Al-Air batteries is greatly diminished. Aluminium suffers from a parasitic corrosion reaction which results in coloumbic losses during discharge of the battery and a loss of fuel during standby.

$$2Al + 6H_2O = 3H_2 + 2Al(OH)_3 \qquad (1.11)$$

In general this reaction is thermodynamically very favourable and can only be inhibited by interfering with the kinetics of the reaction. There are several well tested ways of combating open circuit metal corrosion:

(i) Cathodic Protection – making the metal to be protected the cathode of a corrosion cell by moving the potential into that of the immunity region.

(ii) Anodic Protection – making the metal to be protected the anode of the corrosion cell and by applying a current, move the potential into the passive region.

(iii) pH/Electrolyte choice – choosing the electrolyte/pH of the solution used can bring the metal into the passivity or immunity regions.

(iv) Alloying – the use of corrosion resistant alloys, containing elements that produce more corrosion resistant passive films

(v) Coatings – by coating the metal with a substance even more corrosion resistant than the passive film, it is possible to protect against corrosion. The most common organic form of coating used is paint, followed by waxes and grease. Inorganic protection ranges from chrome plates to ceramic coatings.

(vi) Corrosion inhibitors – inhibitors work in several ways. One is by adsorbing on the surface layer producing a more effective barrier against corrosive substances or by providing a buffering action to the environment.

(vii) Control of electrolyte addition – by adding the electrolyte immediately prior to discharge of the cell, thus minimising the time where open circuit corrosion processes are a problem, thus limiting the wasteful corrosion.

1.4.3 Alloying

With aluminium being considered as a possible means of powering electric cars, much work has been done on alloying the aluminium to reduce open circuit corrosion whilst maintaining a high rate of dissolution under battery discharge conditions. It is well documented [14, 33, 34, 36, 52] that the purity of aluminium used makes a large difference in the corrosion characteristics observed. With higher purity aluminium comes better corrosion resistance and an overall improved performance of the system. It is believed that impurities in low-purity aluminium cause increased hydrogen evolution, and hence corrosion [53, 54]. With high purity aluminium having an elevated manufacturing cost compared to commercial grade aluminium a lot of work has been undertaken to improve the performance of commercial grades[32-34, 36, 52, 55]. Cost is a big issue when considering the development on mechanically rechargeable electric cars as large amounts of aluminium are used. In the UAV application, cost is not so much of an issue with relatively small amounts of aluminium being used in each flight. Despite all the work undertaken, high purity aluminium and designer alloys still show much greater resistance to open circuit corrosion than commercial grades.

Many different alloying additives have been examined for use in an Al-Air system. The most common elements that have been studied include: Zn, Sn, Ga, In, and Mg [32, 35, 39-42, 44, 51, 53, 56-65]. The table below shows a brief summary of some of the more important findings from literature published on aluminium alloys as anode materials.

Composition (wt %)	References	Comments
Al (99.61) Sn (0.745)	[62]	Shown to reduce passive region, shifts pitting potential more negative. Shows dissolution peak of Sn.
Al (99.61) Zn (4.92)	[41, 62]	Shifts pitting potential more negative than Al-Sn. Shows dissolution peak of zinc.
Al (99.95) Zn (1-80)	[61]	Around 3-5 wt% of zinc is best for alloying.
Al (99.61) Zn(5.59) Sn (0.685)	[62]	Shifts pitting potential negative a similar amount as Al-Zn. Retardation of dissolution peak due to presence of Sn.
Al (99.61) Ga (0.40) In (0.21)	[41]	High open circuit potential, minimum anodic polarisation, good anode efficiency, and minimum corrosion rate.
Al (99.61) In (0.77)	[41]	Shows higher corrosion rates compared to other alloys tested against including 5N purity Al.
Al (99.999) In (0.0074)	[53]	Alloying does not improve noticeably the corrosion characteristics over normal Al.
Al (99.61) Mn (5.15)	[41]	Increased corrosion rate and hydrogen evolution over 5N purity aluminium. Slightly lower than that for Al-In.
Al (99.61) Mg (5.57)	[41]	Shows slightly higher corrosion rate than 5N Al, Al-Ga-In and Al-Zn alloys.
Al (99.999) Sn (0.1) Mg (0.5)	[52]	Used for the ALCAN air-battery Shows good corrosion characteristics when tested against commercial grade Al.
Al (-) Si (7/11/22)	[46, 63]	Shows no benefits in corrosion characteristics than unalloyed Al.

Al (-) Zn (4.91-5.25) In (0.029-0.043)	[44, 66]	Negative shift in pitting potential. Zn and In together produce greater enrichment of the oxide film with In.
Commercial Graded Alloys 2S, 3S, 26S, 57S	[32-34, 36]	Corrosion rate: 3S>2S>26S>57S>High-purity Al.

Table 1.11 - A brief summary of key findings from the literature base.

It will be clear that the conclusions from different programmes can be different and there is certainly no general agreement as to the most suitable alloy for this type of application. Tin is one of the more favoured alloying elements under investigation for aluminium alloy-air batteries. Tin is known as an activator species which help to produce super-activation of the aluminium. It has been found that tin accrues at active sites on the alloy surface, weakening the passive layer allowing for extensive dissolution [39]. This sort of activation helps especially in saline solutions where the oxide film is most dominant. Indium and gallium also look interesting alloying elements.

1.4.4 The Oxide Film

In many media the anodic dissolution of the aluminium is hindered by the large overpotentials required due to the presence of a stable oxide film on the surface of the aluminium. The theoretical electrode potential of aluminium without the surface film has been calculated at -1.96 V at pH 7 and -2.37V at pH 14 (both vs. NHE)[8] . In saline solutions the oxide film is stable, thus showing why aluminium appears cathodic to zinc in saline solutions [14]. In strong alkaline solutions hydroxyl ions are able to pit the film [67], producing pathways for aluminium dissolution to occur. In order for the aluminium-air system to be optimised, the oxide film must be modified or removed to lessen the restriction on the aluminium dissolution [16].

1.4.5 The Gelatinous Precipitate

As the dissolution of aluminium continues, the aluminate ion concentration will inherently increase, whilst the hydroxide ion concentration will decrease. This will increase the viscosity and resistivity of the electrolyte and eventually supersaturation will occur and aluminium hydroxide will precipitate out as a hydrargillite phase [19]. The precipitation forces regeneration of hydroxyl ions which in turn decreases the viscosity and resistivity of the electrolyte:

$$Al(OH)_4^- \rightarrow Al(OH)_3 + OH^- \qquad (1.12)$$

Precipitation is most often seen when saline electrolytes (pH < 9) are used. This can cause the electrolyte to gel, which then forms a more crystalline species. Certainly, it is advantageous that an electrolyte is chosen that allows a high solubility of aluminium (III) ions - thus the popularity of concentrated potassium hydroxide.

1.5. A Structural Battery System

With weight being a major factor in the evolution of this battery system and the plane in which it is to be placed, a key area of research is looking into replacing some of the structure of the UAV with the battery itself. The current battery system being used, Li-Polymer batteries, is held within the fuselage pod underneath the wing of the plane. This has several drawbacks including taking up precious volume within the fuselage, and heating the volume of the pod which is not beneficial to the electronics also housed within the pod. By creating a battery that can be used as part of the structure, whilst maintaining the structural integrity of the plane, could solve both weight and heat constraints. This requires the battery to be designed to a specific shape and roughness criteria and involves looking in depth at the structural properties of different areas of the aircraft.

1.5.1 High Surface Area forms of Aluminium

Using high surface area forms of aluminium gives several benefits. It increases the surface area of the anode allowing for much larger currents to be drawn whilst minimising the current density needed. It also allows larger structures with lower weights to be created.

There are various forms of high surface area aluminium which are worth mentioning. Foams and meshes are available commercially for use, whilst other forms of meshes such as fibrous meshes can be easily produced. The main problem arising from the use of meshes and foams is the unavailability of the correct alloys for corrosion-resistant aluminium air batteries. Indeed, often the exact composition is not specified. As stated earlier, the purity of the aluminium makes a big difference to the battery's performance – high purity aluminium does not make good structural foams and meshes due to its inherent softness and malleability. Elements such as magnesium and zinc help to alter the structural properties of the aluminium but most foams and meshes are only available in the pre-determined alloy mixes, using lower purity aluminium. This is partly because of demand, and partly because of the higher associated cost when producing high purity aluminium.

Some research has been done into producing aluminium alloy foams from non-commercial alloys as well as commercial alloys [68-74] with a lot of success. However, presently we

were not able to reproduce any of the methods used in the literature due to a lack of suitable facilities. Some work has been undertaken to examine the feasibility of compressing the best of the commercially available alloys to make compressed foams[71, 75] as well as testing the compressive, tensile and shear stress of many pre-existing foams [76, 77].

Alloying Element	Effects on Structure
Gallium	Usually present at levels of 0.001 – 0.02% - no mechanical effect At 0.2% affects corrosion characteristics. Can lead to grain separation
Indium	0.05 – 0.2% marked influence on the age hardening – increased strength
Magnesium	Markedly increases strength without losing ductility Up to ~ 8 wt% increases yield strength
Manganese	Used to increase strength and control the grain structure Increases yield strength and tensile strength up to 1 wt%
Tin	Increase in strength.
Zinc	With small additional alloying offer the highest combination of tensile properties. (Mg) Largest change in Yield and Tensile strength from 2 – 6 wt%
Iron*	Good strength & ductility at room temperature, and retain strength at elevated temperatures. (especially with additions of Manganese)

Table 1.12 – A table showing many of the possible alloying elements and their effect on the structural strength of the alloy. * iron is one of the most common impurities in low purity aluminium[78].

One of the main objectives of this study is to look into the feasibility of producing a three-dimensional battery structure using a foam/compacted mesh anode. It should provide equivalent structural strength to the existing polymers being used and the battery may have to be any number of different shapes depending on the positioning on the plane. The high

surface area investigations are hoped to help decrease the weight of the battery system, as well as increase the area open to solution, and provide greater structural strength.

2. Experimental Method

2.1 Sources of Chemicals

Deionised water from a Whatman Analyst unit was used throughout all experiments. KOH solutions were made using laboratory grade solid potassium hydroxide pellets from Fisher Scientific, which were dissolved slowly in distilled water within a conical flask. NaCl solutions were made in the same way using laboratory grade solid sodium chloride crystals from Fisher Scientific.

Oxygen and Nitrogen, when needed, were supplied by BOC gases in compressed cylinders and pumped through the standard laboratory pipe system.

2.2 Aluminium Sources

Alloy	Composition (wt %)	Suppliers	Structure	Dimensions (mm)
High Purity Aluminium +	99.999%	Goodfellows	Wire	1 (diameter)
AB50V alloy *	Al 98.30% Mg 0.39% Sn 0.10% Ga 0.05%	Private Suppliers	Sheet	1 (thick)
Chandlery Anode*	Al 94.47% Zn 5.25% Ga 0.02%	MGDuff	Block	Turned Rods: r = 2mm
SAFT Anode *	Al 97.9% Zn 0.11 % Ga 0.10% Fe 0.09% Si 0.08%	dstl	Cylinder	Turned Rods: r = 2mm
Goodfellow/ ERG Foams +	98.5% Al 0.7% Si 0.8% Mg	Goodfellow / ERG	Foam	2cm x 1/2cm x 1/2 cm
Aluminium – Magnesium +	95% Al 5% Mg	Goodfellow	Sheet	25mm x25mm x 0.03mm
Meltspun Aluminium +	Al 94.5% Si 3% Fe 2.5%	Fibretech	Meltspun Fibres	Non-uniform, ~ 0.1 mm diameter

Table 2.2.1 – A Table showing the composition analysis of all the samples used in the experiments included in this report.

**** analysis by Analytical Data Services Ltd***

+ analysis provided by supplier

2.3 Testing Cells

2.3.1 Cell for Voltammetry

The cell is a three electrode, two compartment cell. The reference electrode used is a commercial saturated calomel electrode connected via a Luggin capillary to the working electrode compartment. Also in this compartment is the counter electrode (a platinum mesh), and the working electrode (either an aluminium wire or a small piece of aluminium sheet). This small piece of sheet was soldered using a soldering iron and tin-zinc solder directly onto a length of copper wire above the solution line. This cell is connected to an EG&G potentiostat/galvanostat (See *Table 2.4.1)*, which in turn is connected to a home-built computer system running LabView software that allows data to be presented as current density vs. potential plots. A standard volume of 25 ml electrolyte, room temperature, and air-equilibrated solution was used unless stated otherwise. If deoxygenation was required, nitrogen gas was sparged through the system using the glass tubing and sinter at the base of the cell. Figure 2.3.1 shows a schematic of the cell used.

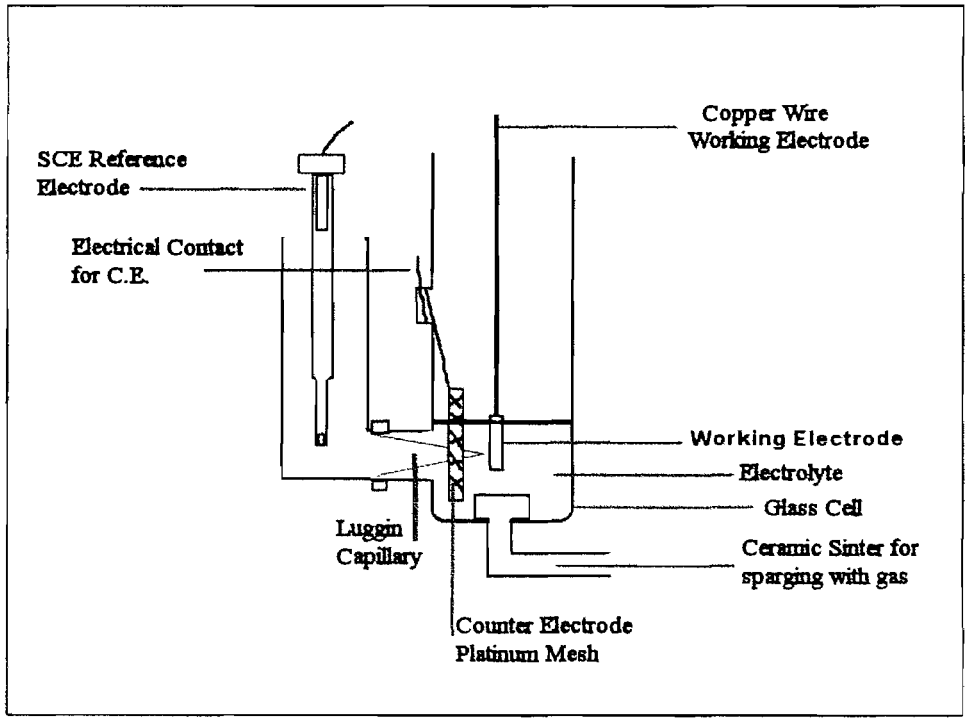

Figure 2.3.1 – Schematic of classical three electrode, two compartment cell used for electrochemical experiments.

2.3.2 Test Battery Cell

In order to achieve a more realistic guide to how the battery system will perform; the Al anode is coupled to an air cathode (*See Table 2.4.1)* in a test battery cell. *Figure 2.3.2* shows the constituent parts of the cell as well as a schematic of how it fits together.

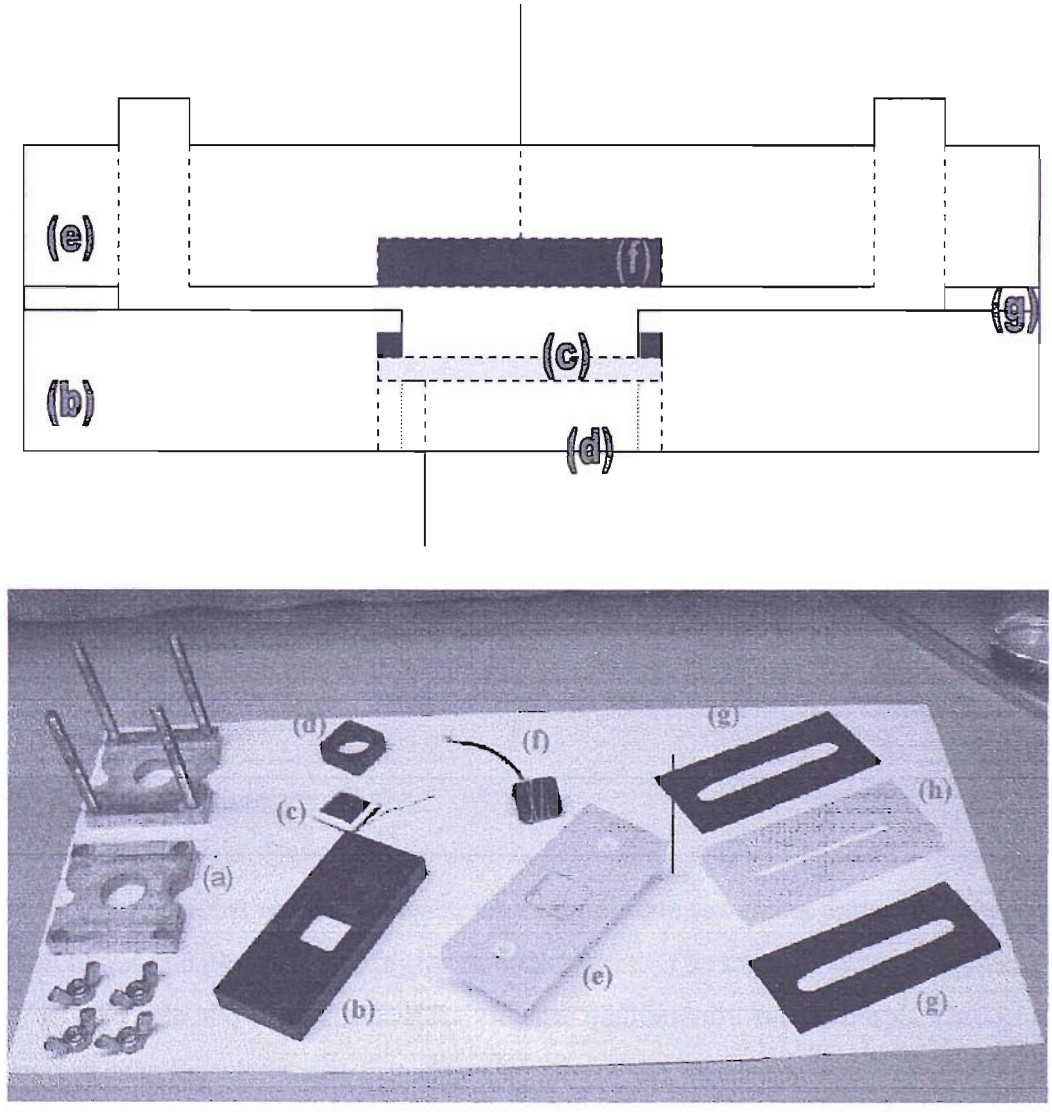

Figure 2.3.2 – Image showing the constituent parts and how they fit together of the test battery cell.

The parts shown in *Figure 2.3.2* are as follows:

(a) Steel vice for clamping the cell together and to provide pressure to force a good seal. This was tightened using four butterfly nuts.
(b) Black polymer block to hold air cathode.
(c) Air cathode with white rubber gasket to prevent leakage, and platinum wire electrical contact. The air cathode was Pt-catalysed carbon supplied by De Nora – North America.
(d) Hollowed polymer block to allow a good seal with air cathode gasket, whilst still allowing air flow to the cathode.
(e) Polymer block to hold anode containing two tubes to allow the flow of electrolyte through the cell.
(f) Carbon block with wire glued to the back (electrical contact tested) which allows for electrical contact to the aluminium anode. The aluminium anode is either wound around this block if in wire form, or held by one of the rubber gaskets onto the carbon block. This was found to give a good electrical contact between the aluminium and the carbon block.
(g) Black rubber gaskets to provide seal between polymer blocks whilst allowing flow of electrolyte through cut-out channel.
(h) Additional spacer polymer block to increase electrode gap / electrolyte volume if needed.

2.3.3 Compression testing

Various lay-ups of wires/fibres were compressed using an Ingstrom compressor up to 100kN. The samples were made up in their appropriate structures then placed between two steel plates and placed in the Ingstrom compressor. The samples were compressed at a rate of 10 kN / min and were checked for strength qualitatively every 10 kN. The compressed samples were made from 5 cm lengths of the meltspun fibre/wires giving a sample size of 5cm x 5cm. The depth varied with the number of layers and the pressure at which they were compressed.

2.4. Instrumentation & Software used

Equipment / Software	Make	Model	Notes
Potentiostat/Galvanostat	EG&G	263A	Connected to Home Built computer
Home-built computer	Home-build	-	-
LabView Software	LabView	V1.5	o/s = Windows 98
Load Cell	Kikusui	PLZ164WA	165W / 0-150 V / 0-33 A
Sigmaplot Software	Sigmaplot	V8.02	o/s = Windows XP
Water Distillation Unit	Whatman	Analyst	-
Electronic Scales	Sartorius	MC1	-
ESEM	Philips	XL	-
Air Cathode	De Nora North America	-	10% Pt loaded

Table 2.4.1 – Table showing Make & Model of all equipment/software used in experimentation.

3. Results

3.1 High Purity Aluminium in KOH

High purity aluminium was tested in wire format (area ~ 0.1 cm^2) in 8M KOH. Gas evolution due to the reaction,

$$2Al + 6H_2O \rightarrow 3H_2 + 6OH^-$$

commenced as soon as the aluminium was placed in the solution. The open circuit potential was measured as -2.10 V versus SCE, using the classical three electrode cell and a digital voltmeter. After an hour on open circuit in 8M KOH at a temperature of ~294 K a SEM image was taken. This is shown in *Figure 3.1.1*, which also shows an image of a wire before immersion into the solution.

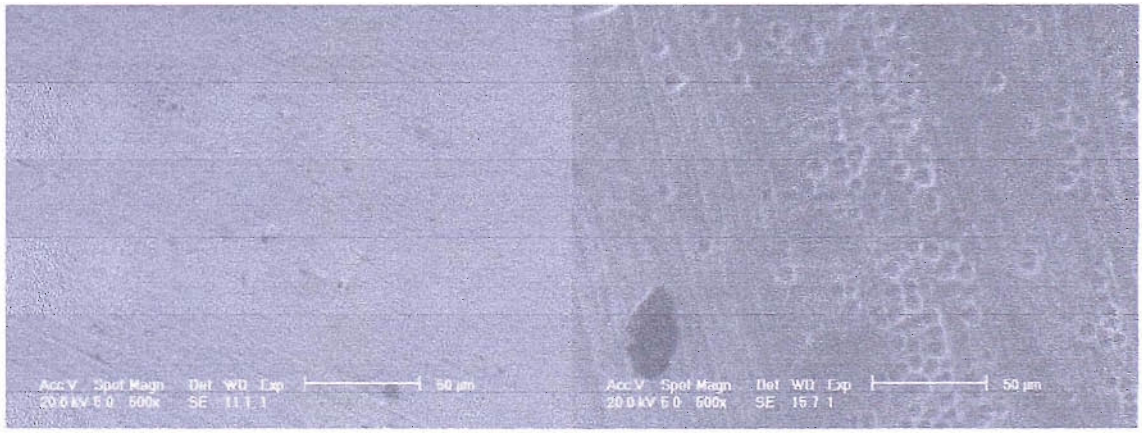

Figure 3.1.1 – SEM data of the surface of a high purity aluminium wire before/after submersion in 8M KOH for 1 hour at a temperature ~ 294K.

Pitting is clearly seen after the wire has been submerged, showing aluminium dissolution from the surface. Thin grooves or scratches are observed in the non-submerged wire and the pitting craters are formed predominantly along these scratches.

The presence of oxygen in solution can lead to a small cathodic current for oxygen-reduction, increasing the rate of corrosion and forcing the open circuit potential more

positive. Removing the oxygen from solution should eliminate this current, shifting the open circuit potential more negative and reduce the wasteful corrosion of the aluminium. This could lead to a way of extending the storage life of the battery, if the change in corrosion rate is significant. By deoxygenating the electrolyte and sealing the battery to exterior oxygen supply until deployment the loss of aluminium would be decreased. Deoxygenation was achieved by sparging the solution with dry nitrogen gas for 30 minutes before testing. The wire was then submerged in 1M KOH electrolyte and was continuously sparged with N_2 for a period of one hour at a temperature of ~ 294 K. Hydrogen evolution was still observed. SEM images were then taken of the surface of this wire and of a wire submerged for the same time in an air-equilibrated solution of 1M KOH. *Figure 3.1.2* shows the SEM images taken.

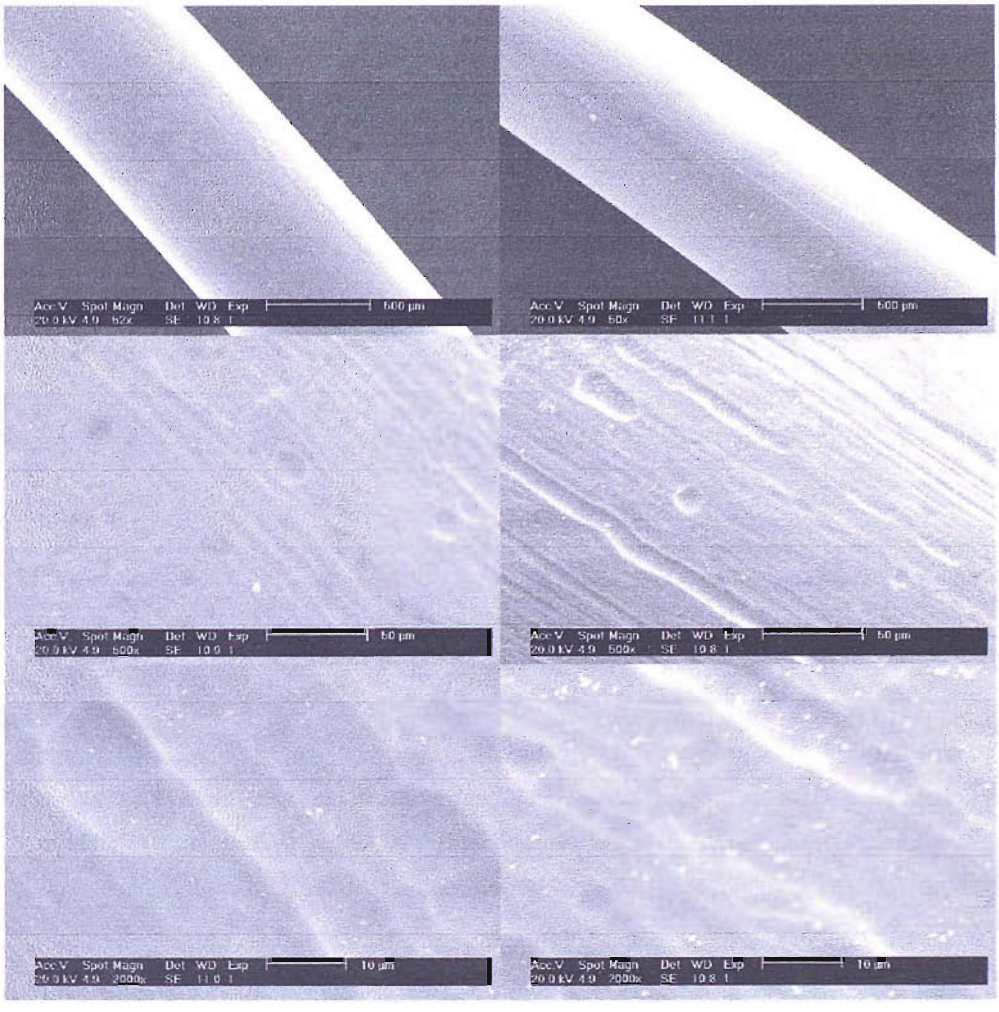

Figure 3.1.2 – SEM photos of high purity aluminium samples submerged in air-equilibrated and deoxygenated solutions of 1M KOH for 1 hour. The left hand column of three images shows the deoxygenated solution, whilst the right hand column shows the air-equilibrated solution.

It is clear from *Figure 3.1.2* that pitting occurs to similar extents in both the deoxygenated and air-equilibrated solutions. In order to confirm whether any significant difference occurs voltammetry of high purity aluminium wires was carried out in both deoxygenated and air-equilibrated solutions. The aluminium wire was submerged in solution after deoxygenation and the voltammagram ran immediately after. Scans were started at -2.5 V vs. SCE, and ramped to 0.0 V at a scan rate of 50 mV s^{-1}, and temperature of ~ 294 K. *Figure 3.1.3* shows voltammagrams for high purity aluminium in air-equilibrated and deoxygenated electrolytes of 1M KOH.

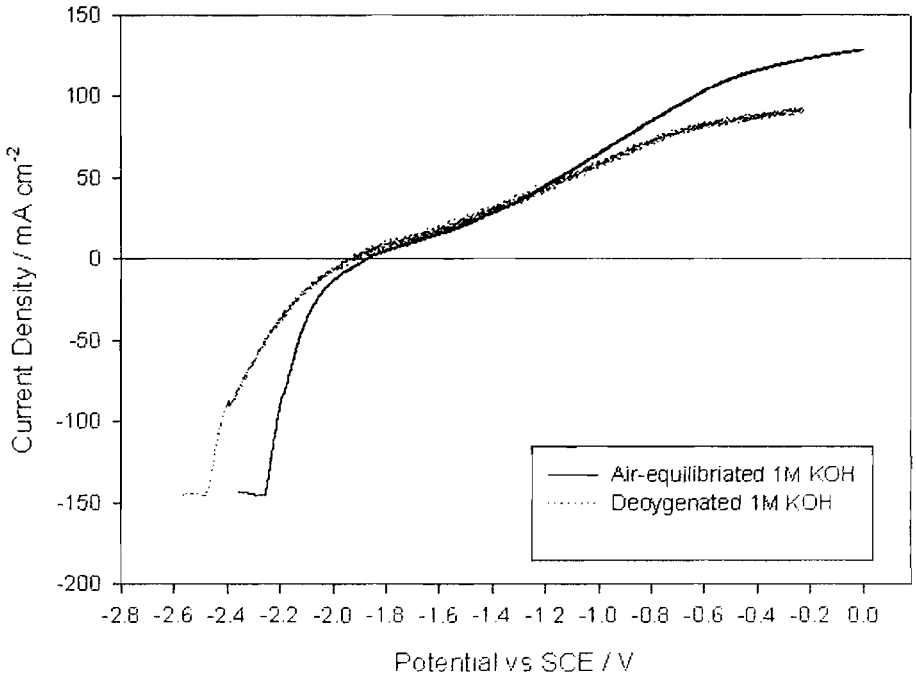

Figure 3.1.3 – Voltammetry data obtained for 5N purity aluminium wire (area ~ 0.1 cm^2) in air-equilibrated and deoxygenated 1M KOH solutions at a scan rate of 50 $mV\ s^{-1}$, and a temperature of ~294 K.

Negative of the open circuit potential, in both cases, there is a large cathodic current from hydrogen evolution. Positive of the open circuit potential the anodic aluminium dissolution current steadily rises reaching a plateau at around 100 mA cm^{-2}. The corrosion resistance between ± 10 mV is ~ 9 Ω cm^{-2} is consistent with rapid open circuit corrosion. It is clear from the graph that there is a small shift in the open circuit potential in the negative potential direction when the solution is deoxygenated; but on the current density scale shown, a clear cathodic current density for oxygen reduction cannot be observed. The negative shift of the open circuit potential is small, so it is deemed to have little effect on the corrosion characteristics of the sample. All this data reinforces the conclusion of the SEM images; contact with air has little effect on the rate of corrosion on open circuit.

To help to quantify the rate of corrosion of the high purity wire, mass loss experiments were undertaken. High purity aluminium wire (0.273 g) was submerged in 25 ml of 8M KOH until it had dissolved. At given time periods the wire was removed, washed using

distilled water, dried, weighed, and then returned to the 8M KOH solution. *Figure 3.1.4* shows the results of the mass loss experiment.

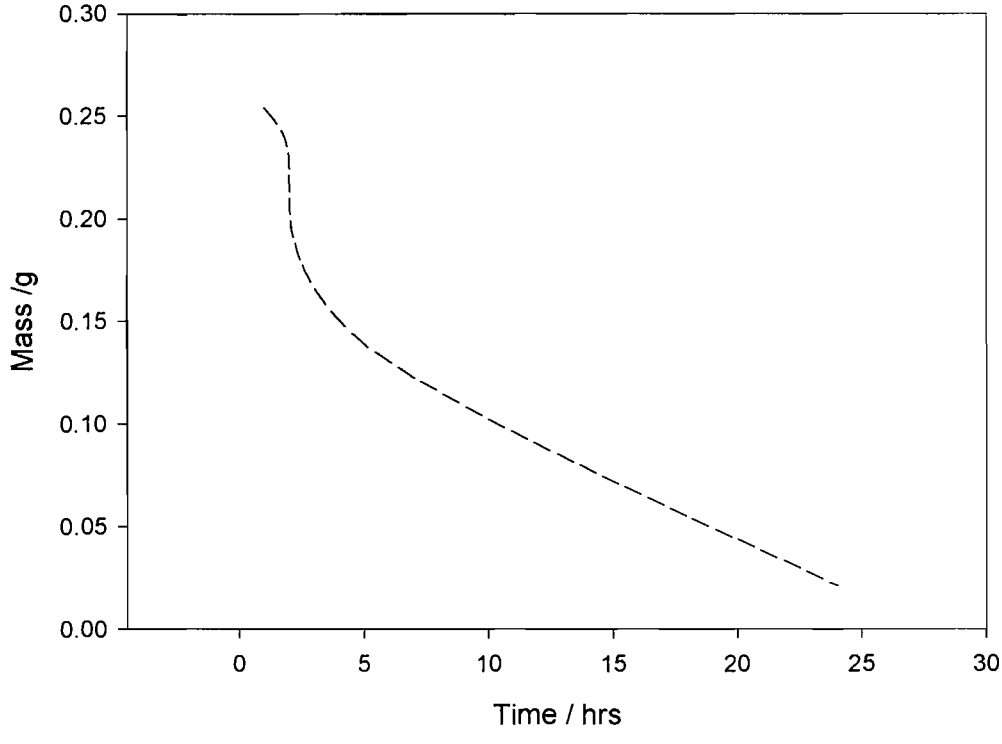

Figure 3.1.4 – Mass loss data for 0.273 g of high purity aluminium submerged in 25 ml of 8M KOH at a temperature of ~ 294 K. The wire was removed from solution, washed, dried and weighed, before being returned to the solution.

The high purity aluminium wire can be seen initially to lose weight rapidly but after the loss of ~ 40 % of its initial weight, the rate of loss decreases. It is almost entirely dissolved within the 24 hour period. The rate of mass loss is inextricably linked to the surface area of the aluminium open to solution. This could explain the fast initial mass loss rate which then slows down as the surface area open to attack decreases. Passivation of the surface could also explain the sudden drop in mass loss rate with time. With an ideal situation being to store the aluminium battery for a timescale of months before flight, we can see that this system would not be suitable unless the electrolyte is added immediately prior to flight. Voltammetry data was obtained for the aluminium in 8M KOH.

Scans were started at -2.3 V vs. SCE, and ramped to 0.0 V at a scan rate of 50 mV s^{-1}, and temperature of ~ 294 K.

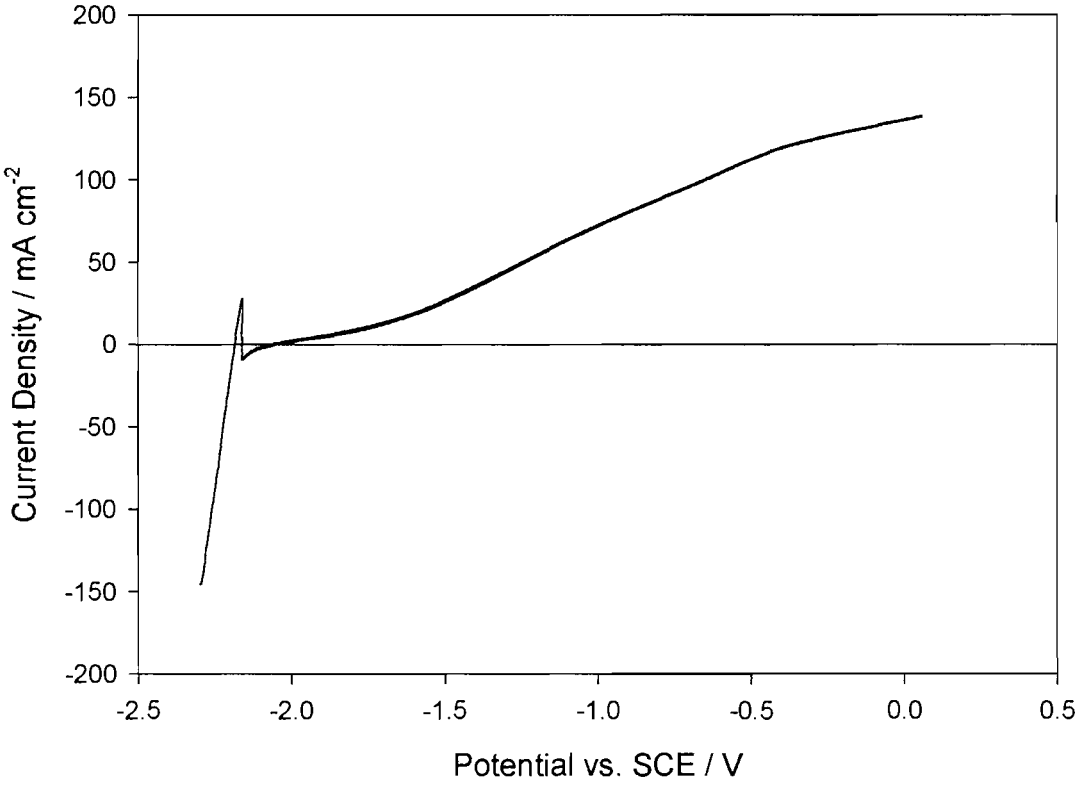

Figure 3.1.5 – Voltammetry data obtained for 5N purity aluminium wire (area ~ 0.1 cm^{-2}) in 8M KOH solution at a scan rate of 50 mV s^{-1}, and a temperature of ~ 294K.

From *Figure 3.1.5* the open circuit potential can be read as ~ -2.1V vs. SCE, close to the value in 1M KOH. There is a large cathodic current present at potentials negative of the open circuit potential. This results from hydrogen evolution and is confirmed by gas being observed evolving from the electrode during the experiment. Immediately positive of the open circuit potential an anodic current is observed and this increases as the overpotential is increased – reaching ~ 130 mA cm^{-2} at 0 V. The rate of anodic dissolution in 1M KOH and 8M KOH is similar. The peak observed immediately negative of the open circuit potential (around -2.2 V) is reproducible but, as of yet, unexplained.

Using the classical three electrode cell, tests were undertaken to examine how constant the potential was at a given current density over the period of 1 hour (the original flight time aim). Constant current densities of 30, 85, and 120 mA cm^{-2} we used. These were thought to be indicative of possible operational current densities.

High purity aluminium wire was tested (area ~ 0.1 cm^2) in 8M KOH. The data can be seen below in *Figure 3.1.6.*

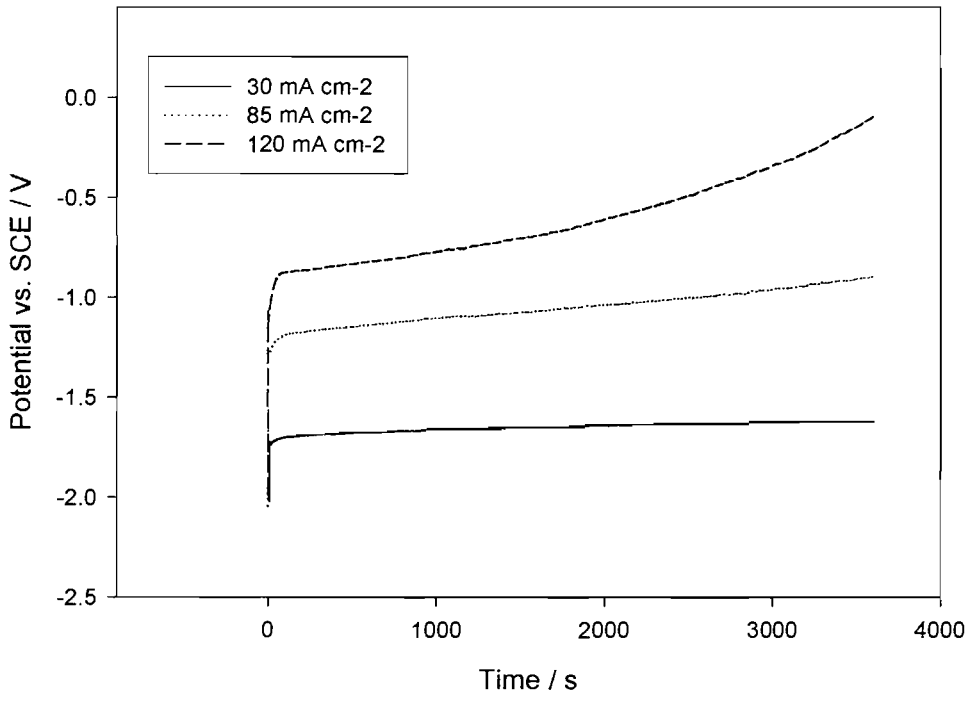

Figure 3.1.6 – Graph showing Potential vs. SCE / V versus Time /s for high purity aluminium wire held at three different current densities: 30, 85, and 120 mA cm^{-2}, in 8M KOH at ~ 294 K.

It is clear to see from *Figure 3.1.6* that a reasonably constant potential is observed over the one hour period in both the lower current density curves. Moreover, the steady potentials at the lower current densities are sufficiently negative to be optimistic of a satisfactory battery voltage when the aluminium anode is combined with an air cathode. At 120 mA cm^{-2} the potential becomes more positive by about 0.5 V over the one hour period. The computer program being used to obtain the data allows the user only to control the current of the system, not the current density. This means that as aluminium dissolves during discharge and the area of the electrode changes, the operating current density will change, shifting the potential. By measuring the final surface area of the aluminium wire held at

120 mA cm^{-2}, it was possible to show that due to the decreasing area, the current density applied to the wire changes with time, accounting for the rise in potential noted.

By comparing *Figure 3.1.6* with *Figure 3.1.5* it is observed that the constant current experiment produces slightly more negative potentials (by 0.1 – 0.2 V) for corresponding current densities.

SEM analysis was undertaken of the sample of wire held at 85 mA cm^{-2}. *Figure 3.1.7* shows the SEM images.

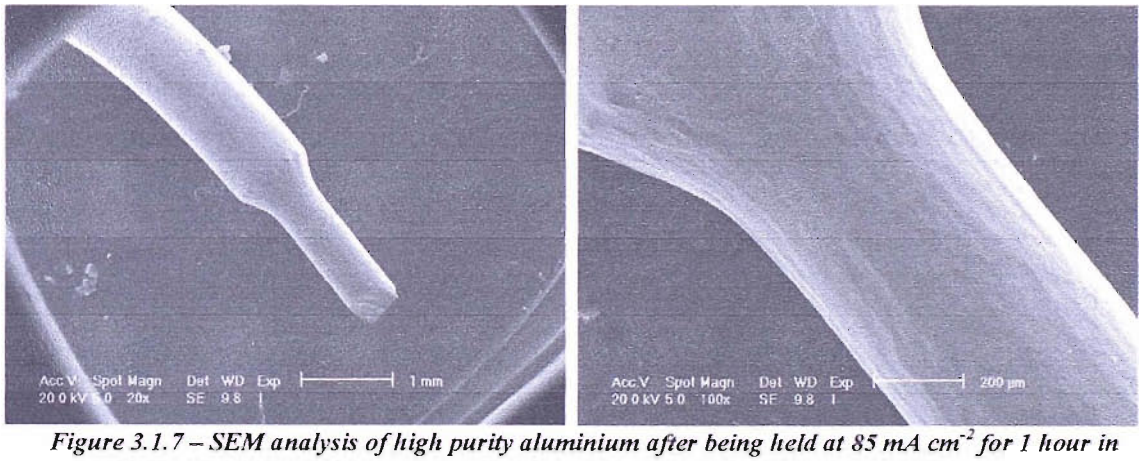

Figure 3.1.7 – SEM analysis of high purity aluminium after being held at 85 mA cm^{-2} for 1 hour in 8M KOH

The SEM analysis shows very smooth dissolution of aluminium over the entire surface of the wire submerged in solution. The thicker region of the wire corresponds to the wire above the solution level. An estimate of the concentration of Al(III) in solution after the experiment is ~ 40 mM (~0.4 wt% Al_2O_3).

3.2 High Purity Aluminium in NaCl

Submergence of high purity aluminium wire in 2M NaCl under open circuit conditions leads to no noticeable gas evolution. The open circuit potential was measured to be -1.75 V vs. SCE, using a digital voltmeter. Zero mass loss over a 48 hour period was observed when the wire was submerged in 2M NaCl. *Figure 3.2.1* shows the voltammetry of high purity aluminium wire in 2M NaCl. The scan was started at -2.3 V vs. SCE, at a scan rate of 50 mV s^{-1}, and at a temperature of ~ 294 K.

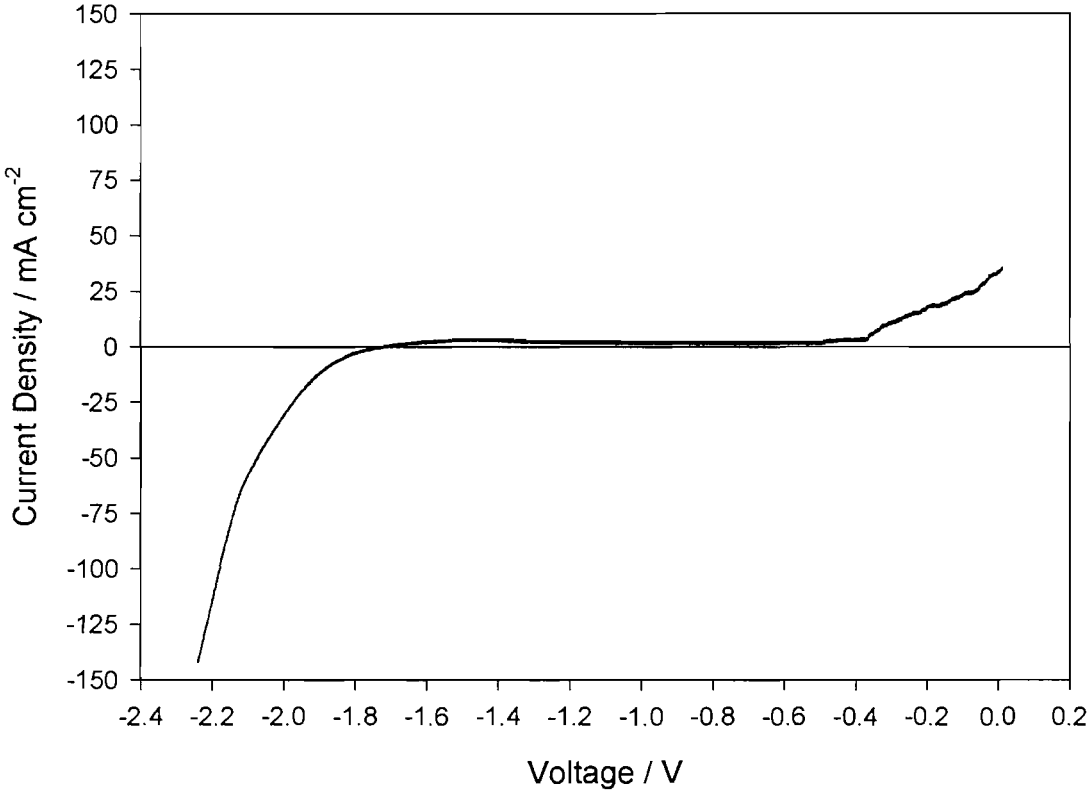

Figure 3.2.1 – Voltammetry data obtained for 5N purity wire (area ~ 0.1 cm^2) in 2M NaCl solution at a scan rate of 50 mV s^{-1}, and a temperature of ~ 294 K.

The open circuit potential can be read from *Figure 3.2.1* as ~ -1.7 V vs. SCE, which agrees with the result from the digital voltmeter. Compared with the high purity aluminium in

8M KOH, there is still a large cathodic current present at potentials negative of the open circuit potential, but there is a wide potential range where there is only a very low current and an overpotential of ~ 1.3 V needs to be applied positive of the open circuit potential in order to get significant aluminium dissolution. The anodic current never gets above ~ 40 mA cm^{-2} in the range tested. Also the very low slope of the voltammagram through the open circuit potential is consistent with the absence of corrosion on open circuit.

Over the period of an hour, a constant current was applied to the wire in 2M NaCl, and the potential measured. The samples were held at 30, 85 and 120 mA cm^{-2}. The data can be seen below in *Figure 3.2.2.*

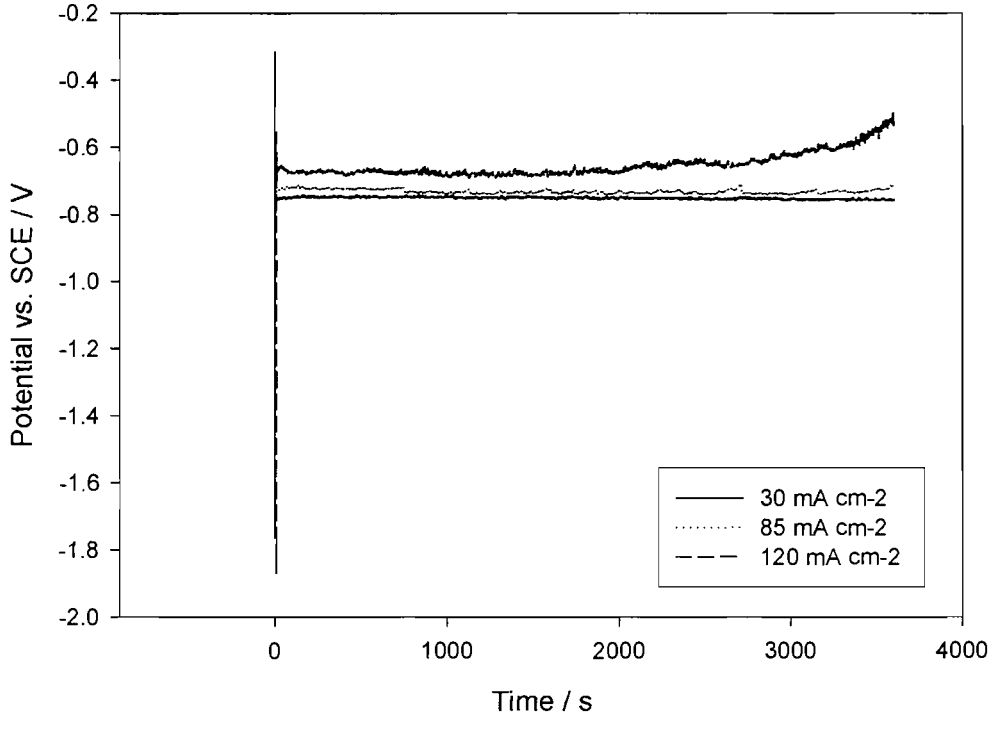

Figure 3.2.2 – Graph showing Potential vs. SCE / V versus Time /s for high purity aluminium held at three different current densities: 30, 85, and 120 mA cm^{-2}, in 2M NaCl at ~ 294 K.

At all current densities, the aluminium takes up a potential close to – 0.7 V; a value that is unlikely to give a useful voltage from an al-air battery. It is clear that at the lower current densities a constant potential is observed over the hour long period. For the higher current a slight rise (~ 0.1 V) is observed at the end of the hour. Area measurements after the

experiment confirm that the decrease in surface area can account for this change in potential, hence some dissolution is occurring. The three different current densities fall within a very small potential range showing that the anodic current must rise rapidly over a small potential range. If we compare this with *Figure 3.2.1*, we can see that at ~ -0.7 V (where the three current densities lay) no anodic current is seen to flow. This shows that the constant current measurements do not agree entirely with the voltammetry of the system; clearly the I/E relationship depends on the experimental approach.

SEM analysis was undertaken of the sample of wire held at 85 mA cm^{-2}. *Figure 3.2.3* shows the SEM images.

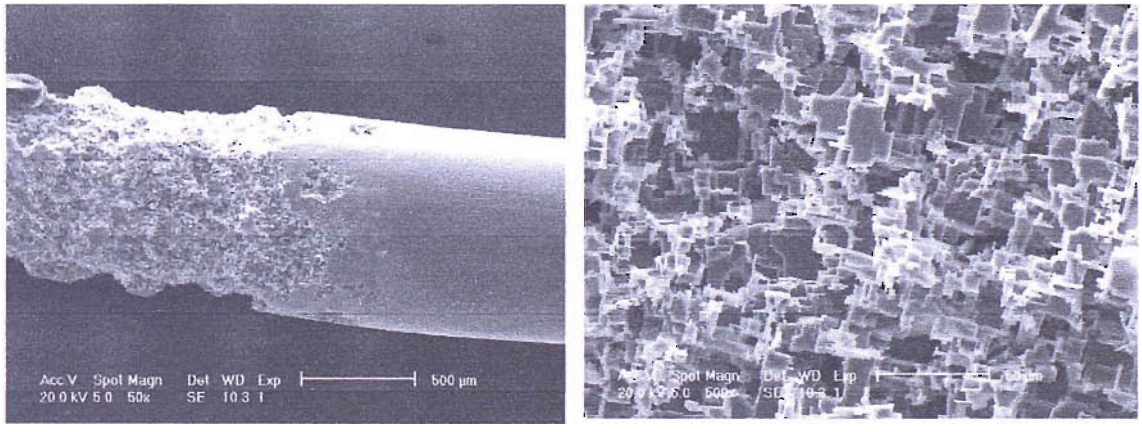

Figure 3.2.3 – SEM analysis of high purity aluminium after being held at 85 mA cm^{-2} for 1 hour in 2M NaCl

The SEM images seen in *Figure 3.2.3* show a much less uniform corrosion than in 8M KOH and a highly complex structure present on the surface of the aluminium. This structure is believed to be alumina based. Further tests need to be carried out to verify the chemical composition of the structure. Certainly, the Al(III) is not soluble in chloride media.

3.3 AB50V Aluminium Alloy in 8M KOH

The AB50V alloy with major alloying components of Mg, Sn, and Ga, was tested in sheet form (area ~ 0.1 cm^2) in 8M KOH solution. The open circuit potential was measured using a digital voltmeter as ~ -2.0 V vs. SCE. The sample dissolves rapidly in 8M KOH under open circuit conditions and considerable gas evolution is noted as soon as it is submerged in the solution. Mass loss data confirms this high rate of corrosion (See *Figure 3.3.1*). Dissolution of 0.453 g of AB50V is complete in 2 days.

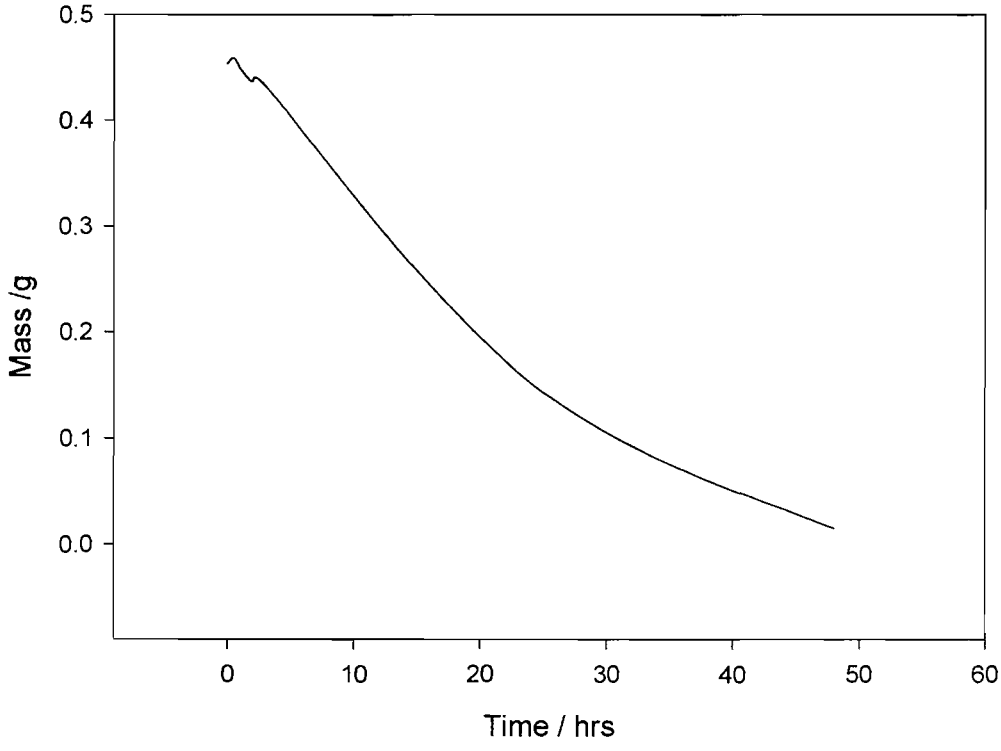

Figure 3.3.1 – Mass loss data for 0.453g of AB50V alloy submerged in 25 ml of 8M KOH at a temperature of ~ 294 K. The wire was removed from the solution, washed, dried and weighed, before being returned to the solution.

As with high purity aluminium, a large corrosion rate is seen over the testing period, and it is not suitable for a wet storage application.

Voltammetric data was obtained for the system and is shown in *Figure 3.3.2*. Scans were started at -2.3 V vs. SCE, and ramped to 0.0 V at a scan rate of 50 mV s^{-1}, and a temperature of ~ 294 K.

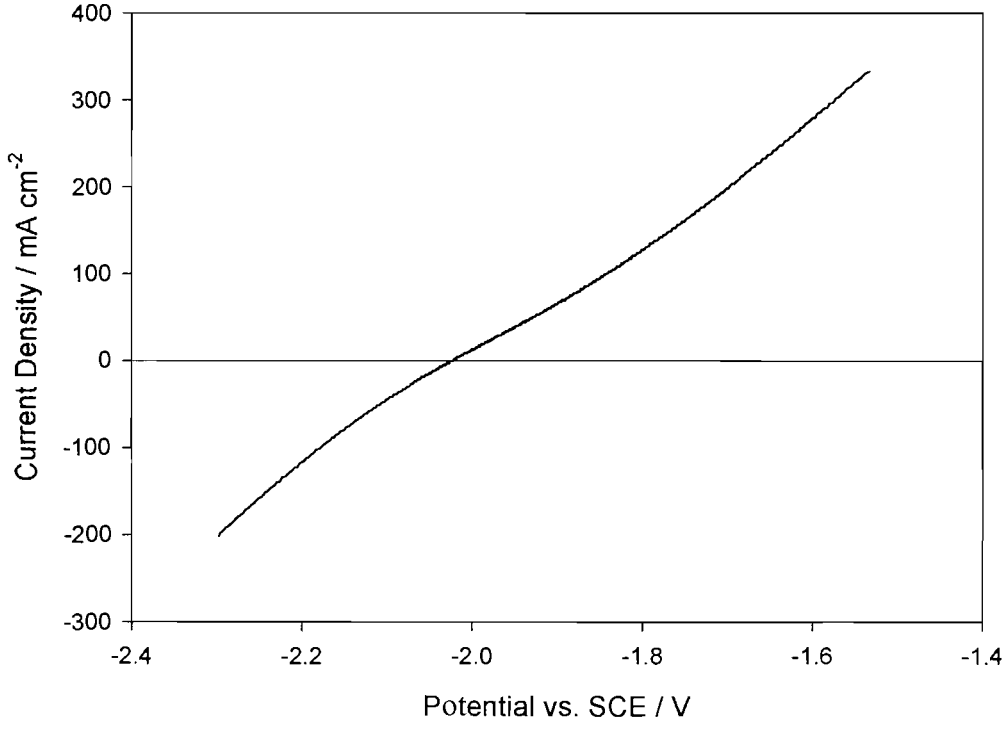

Figure 3.3.2 – Voltammetry data obtained for AB50V alloy sheet (area ~ 0.1 cm^2) in 8M KOH solution at a scan rate of 50 mV s^{-1}, and a temperature of ~ 294 K.

The open circuit potential can be read from the graph as ~ -2.0 V vs. SCE, which agrees with initial measurements. The slope of the I/E response through the open circuit potential shows a considerable corrosion rate. The corrosion resistance is ~ 2 Ω cm^{-2} compared with ~ 9 Ω cm^{-2} for high purity aluminium. Much larger anodic and cathodic currents are observed either side of the open circuit potential than with high purity aluminium. At about -1.6 V vs. SCE, the current density is around 300 mA cm^{-2}; double that seen with high purity aluminium.

Over the period of an hour, the potential was measured when applying a constant current to the system. Current densities of 30, 85 and 120 mA cm^{-2} were used and graphs plotted for each (See *Figure 3.3.3).*

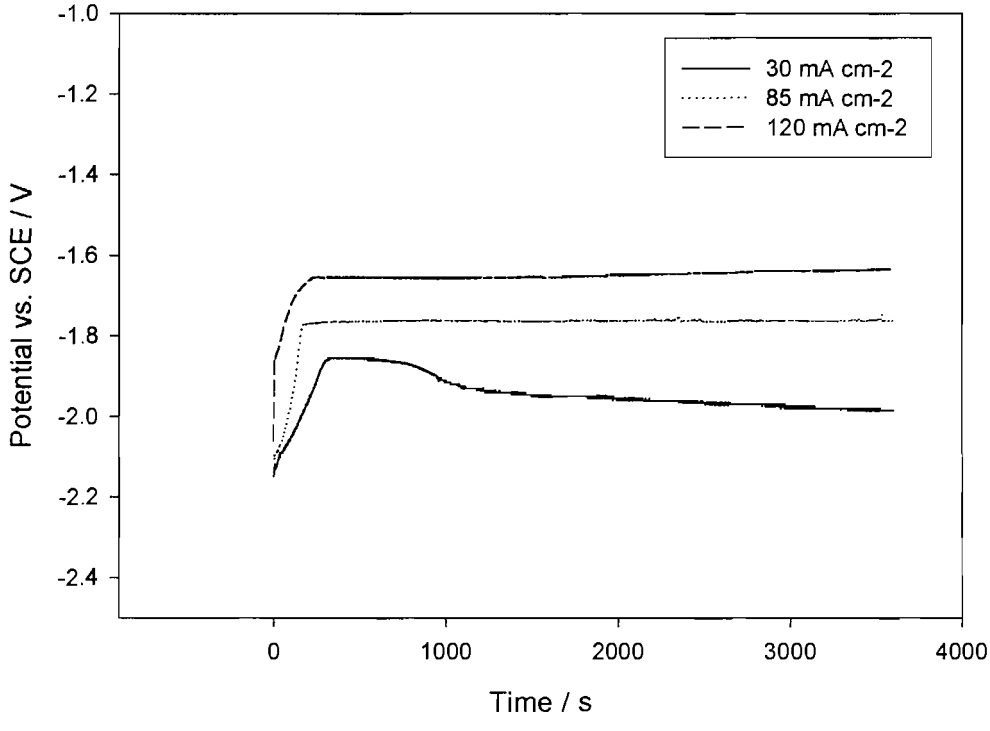

Figure 3.3.3 – Graph showing Potential vs. SCE /V versus Time /s for AB50V alloy sheet (area ~ 0.1 cm^2) held at three different current densities: 30, 85, and 120 mA cm^{-2} for 1 hour, in 8M KOH at ~ 294 K.

The change in potential for all of the high purity aluminium sources held at 120 mA cm^{-2} is not seen in *Figure 3.3.3.* The AB50V alloy is in sheet format, rather than wire, and so small amounts of corrosion will not lead to a significant change in surface area, unlike with the high purity aluminium wire. All of the AB50V samples hold a roughly constant potential over the one hour period. After some initial shifts in potential, the aluminium takes up a steady state potential which is very negative, suggesting that this might be a good alloy for a battery. When compared the corresponding potentials in *Figure 3.3.2*, the potentials are more positive than expected by as much as ~ 0.3 V. Again, the I/E relationship depends on the experimental method.

SEM analysis was undertaken of the sample of AB50V held at 85 mA cm^{-2} (See *Figure 3.3.4)*.

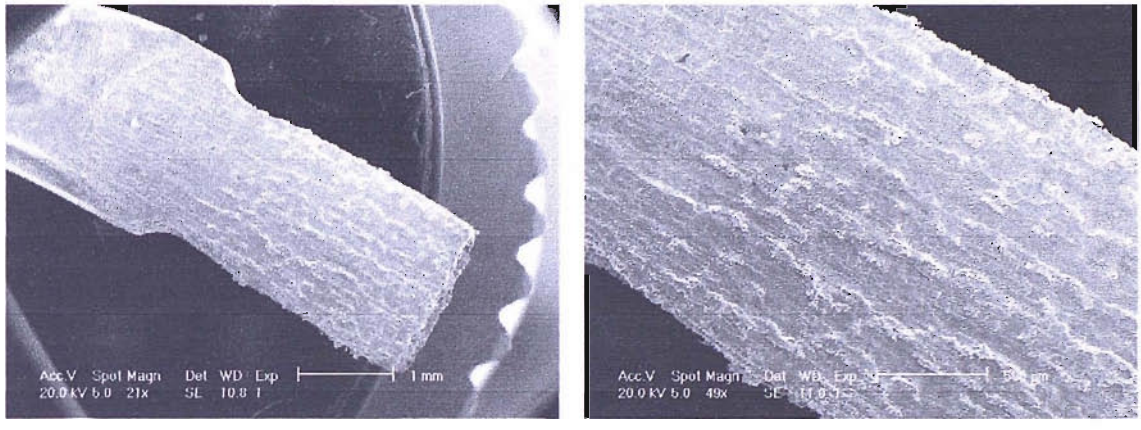

Figure 3.3.4 – SEM analysis of AB50V sheets after being held at 85 mA cm^{-2} for 1 hour in 8M KOH

The SEM images in *Figure 3.3.4* show a much rougher surface of the alloy after aluminium dissolution than with high purity aluminium but not the complex structure observed for pure aluminium in NaCl. With non-uniform dissolution being seen, this could also help to explain why no large change in surface area, hence potential, is observed in the AB50V samples. The rough surface after dissolution could be due to the alloy elemental structure, leaving some areas more prone to corrosion than others.

3.4 AB50V alloy in 2M NaCl

AB50V submerged in 2M NaCl shows no noticeable signs of gas evolution or corrosion, and mass loss experiments over a period of two days lead to negligible changes in mass. Using a digital voltmeter, the open circuit potential was measured as ~ -1.70 V vs. SCE. *Figure 3.4.1* shows the voltammetry of AB50V alloy sheet in 2M NaCl. The scan was started at -2.3 V vs. SCE at a scan rate of 50 mV s^{-1}, and a temperature of ~ 294 K.

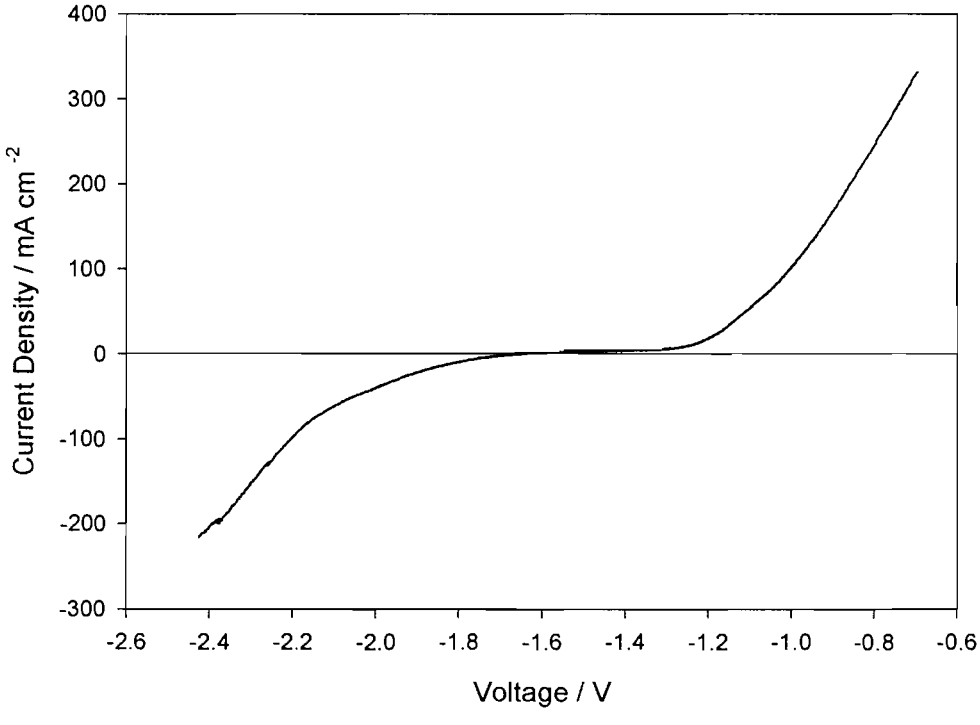

Figure 3.4.1 – Voltammetry data obtained for AB50V alloy sheet (area ~ 0.1 cm^2) in 2M NaCl solution at a scan rate of 50 mV s^{-1}, and a temperature of ~ 294 K.

The open circuit potential can be read from *Figure 3.4.1* as ~ -1.7 V vs. SCE. Negative of the open circuit potential there is still a considerable cathodic current. There is, however, a much larger anodic current present at relatively lower overpotentials (~ 0.5 V), compared with high purity aluminium.

Over the period of an hour, a constant current was applied to the alloy in 2M NaCl, and the potential measured. The samples were held at 30, 85, and 120 mA cm^{-2}. The data can be seen below in *Figure 3.4.2.*

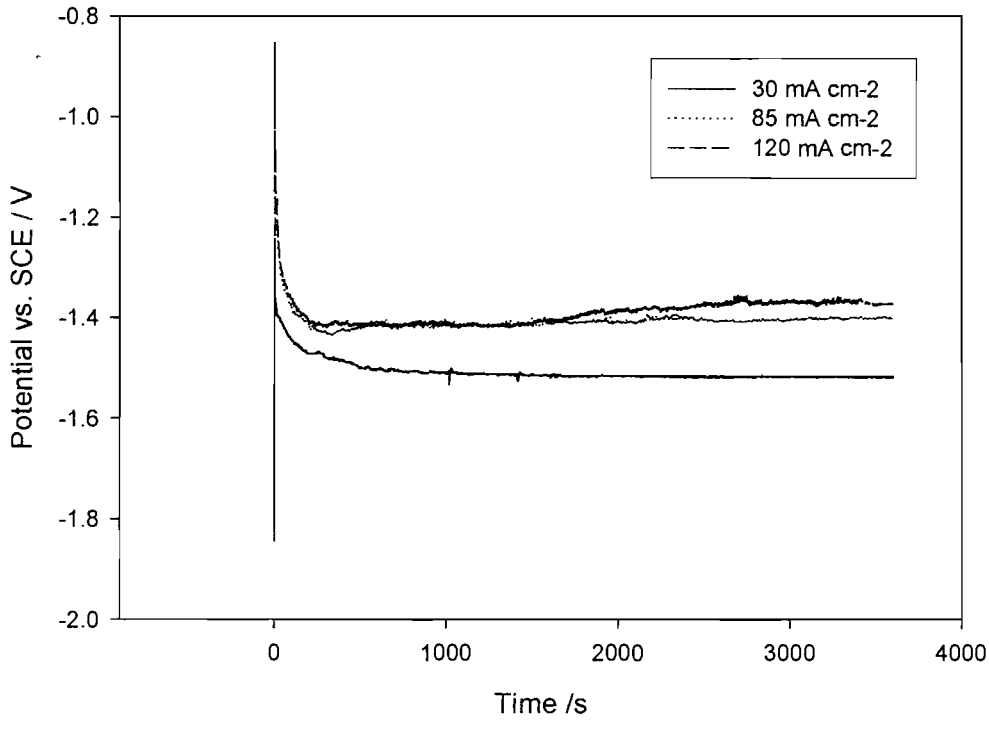

Figure 3.4.2 – Graph showing Potential vs. SCE / V versus Time / s for AB50V alloy sheet held at three different current densities: 30, 85, and 120 mA cm^{-2}, in 2M NaCl for 1 hour, at ~ 294 K.

In *Figure 3.4.2* a roughly constant potential is observed for all three of the current densities and the potential is sufficiently negative to make this an interesting system for battery studies. There is a difference in potential of about ~ 0.1 V between 30 and 85 mA cm^{-2}, but very little between 85 and 120 mA cm^{-2}. This can be seen from *Figure 3.4.1* as the dissolution of aluminium accelerates rapidly with increasing overpotential. The constant current experiment produces potentials more negative by ~ 0.2 V than expected from the voltammetry. SEM analysis was undertaken of the sample held at 85 mA cm^{-2}, which can be seen in *Figure 3.4.3.*

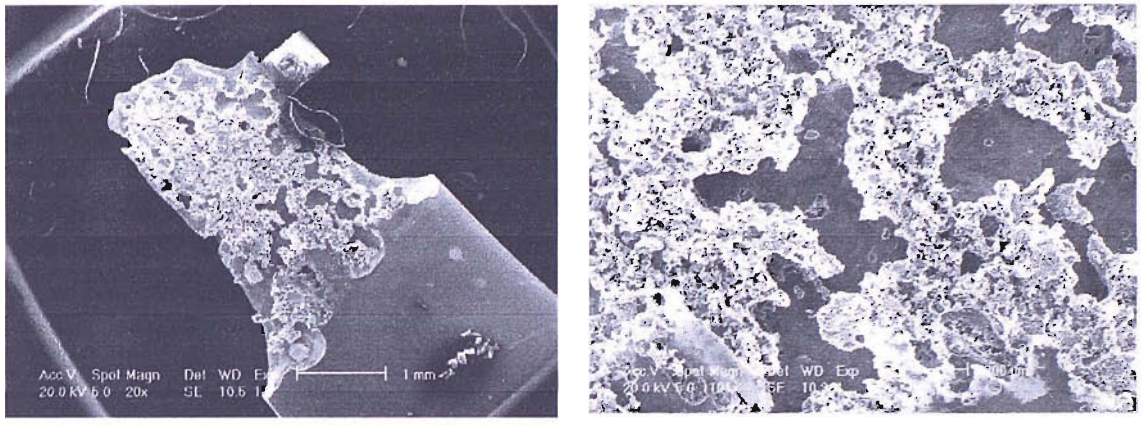

Figure 3.4.3 – SEM analysis of AB50V alloy after being held at 85 mA cm^{-2} for 1 hour in 2M NaCl

The highly complex structure observed with high purity aluminium wire in 2M NaCl, is not observed in *Figure 3.4.3.* although the dissolution is again, non-uniform. A structure is formed on the alloy surface, believed to be alumina based, but it is not as complex as in the high purity aluminium case. Again, further tests need to be carried out to investigate this structure.

3.5 Voltammetry Studies of other Aluminium Alloys

Four other alloys tested during the project will be discussed. These are: meltspun aluminium alloy, aluminium-magnesium alloy, and two chandlery anodes. The exact composition of these can be found in Table 2.2.1. They were all tested in both 8M KOH and 2M NaCl solutions. All the alloys tested corrode on open circuit in potassium hydroxide showing extensive hydrogen evolution.

The meltspun aluminium alloy was supplied in a mat of meltspun fibres. These fibres are created by spinning molten aluminium from a turning wheel. The effect gives an uneven diameter along the threads and can also lead to problems with alloying impurities when trying to produce it with high purity aluminium. In 8M KOH the scan was started from -1.8 V vs. SCE, and in 2M NaCl at -2.4 V vs. SCE. Both were undertaken at a scan rate of 50 mV s^{-1} and a temperature of ~ 294 K (*Figure 3.5.1)*. Because of the uncertain area, the current densities are only estimates.

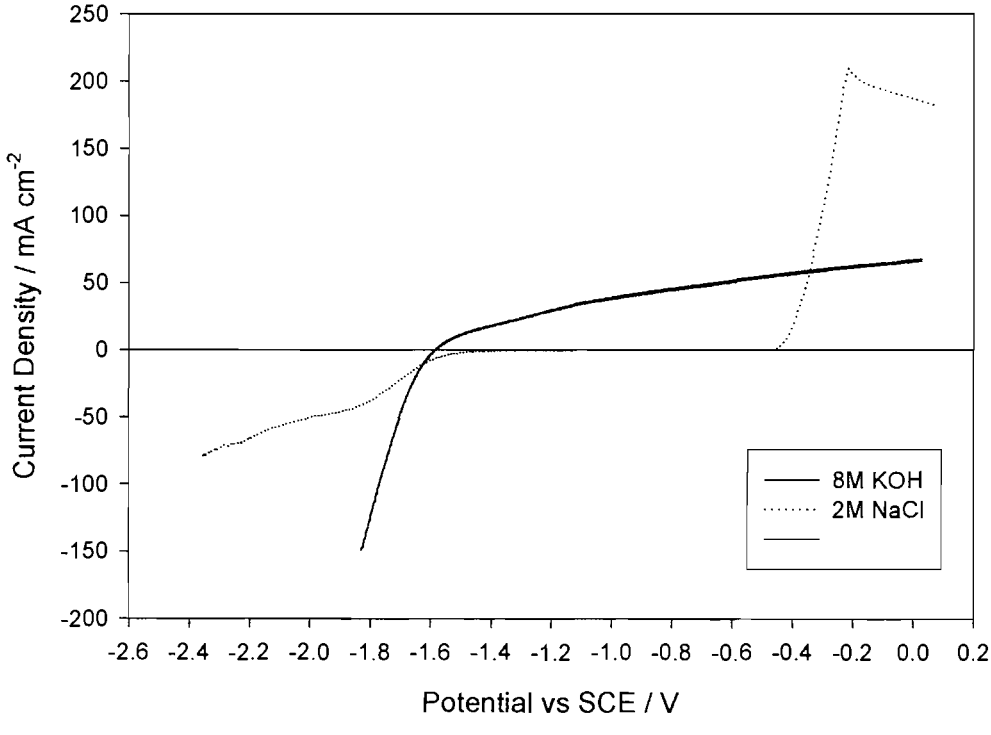

Figure 3.5.1 **– Voltammetry data obtained from meltspun aluminium fibre (area ~ 0.1 cm^2) in two different electrolytes (8M KOH and 2M NaCl). Taken at a scan rate of 50 mV s^{-1}, and a temperature of ~ 294 K.**

A large cathodic current can be observed in *Figure 3.5.1* for meltspun aluminium in 8M KOH. The open circuit potential is -1.6 V and hydrogen evolution occurs significantly positive to previous experiments; the alloying elements are catalysing hydrogen evolution. Positive of the open circuit potential, the anodic current rises slowly, and even at an overpotential of + 1.5 V the current density barely breaks the 50 mA cm^{-2} mark.
In 2M NaCl a considerable rate of dissolution is observed for the aluminium, but only at an overpotential of + 1 V.

The aluminium-magnesium alloy comes in sheet format and is cut down to the correct size and then soldered onto copper wire. This alloy is not ideal for testing how the magnesium content affects the electrochemical characteristics of the aluminium, due to its high concentration in the alloy (5 wt%), but does allow insight into how large alloying elements can effect the sample characteristics. In 2M NaCl the scan was started at -2.4 V vs. SCE, a scan rate of 50 mV s^{-1} and temperature of ~ 294 K (*Figure 3.5.2)*. No voltammagram could be obtained for aluminium-magnesium in 8M KOH due to the almost instantaneous dissolution on contact with solution.

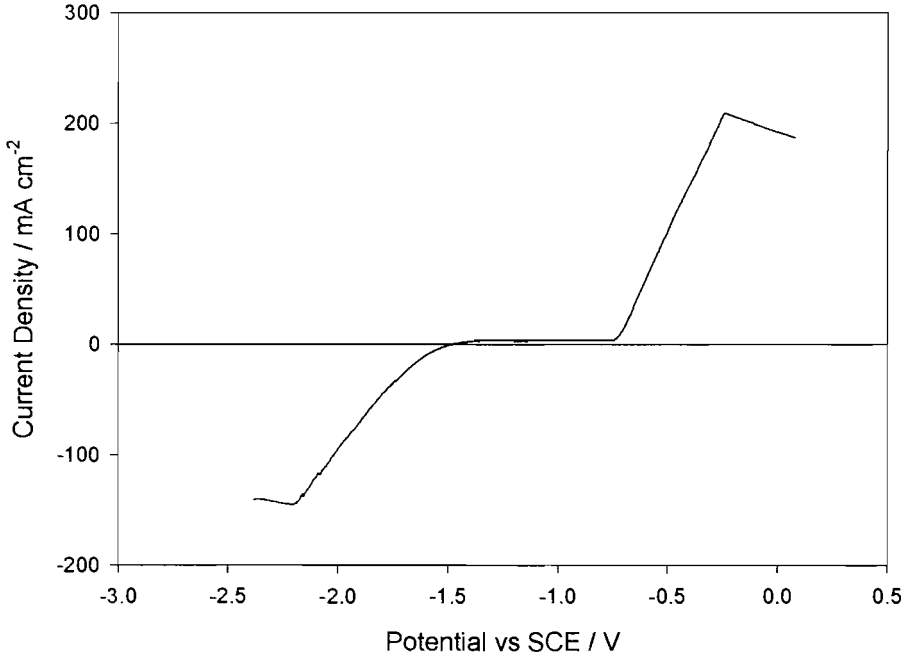

***Figure 3.5.2* –Voltammetry data obtained from aluminium magnesium foil (area ~ 0.1 cm^2) in 2M NaCl. Taken at a scan rate of 50 mV s^{-1}, and a temperature of ~ 294 K.**

Aluminium-magnesium alloy exhibits a large cathodic current immediately negative of the open circuit potential, and a large anodic current at overpotentials of ~ 1 V as seen in *Figure 3.5.2.*

The SAFT anode came as a large cylinder, and small samples were cut out and turned down into 2 mm diameter cylinders for testing. These were then soldered onto a copper wire for electrochemical testing. In 2M NaCl, scans were started from -2.4 V vs. SCE, and with 8M KOH scans were started at -2.0 V vs. SCE. Scan rate was set at 50 mV s^{-1} and it was undertaken at a temperature of ~ 294 K (*Figure 3.5.3).*

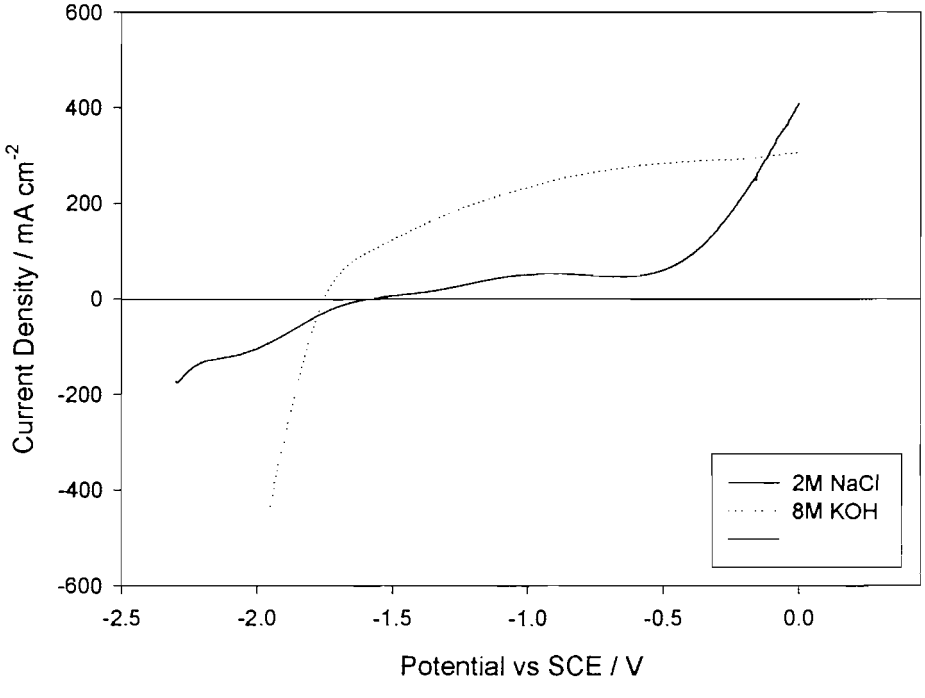

***Figure 3.5.3* - Voltammetry data obtained for the SAFT aluminium anode (area = 0.2 cm^2) in 8M KOH and 2M NaCl solutions at a scan rate of 50 mV s^{-1}, and a temperature of ~294 K.**

A large cathodic current is observed immediately negative of the open circuit potential particularly in 8M KOH in *Figure 3.5.3.* With 8M KOH large current densities are achieved positive of the open circuit potential, but the change in dissolution rate with potential drops off above 100 mA cm^{-2} and at about – 0.5 V vs. SCE the curve starts to plateau at ~ 300 mA cm^{-2}. With 2M NaCl, at small overpotentials moderate current

densities are achieved (~ 50 mA cm^{-2}), but for significant dissolution to occur an overpotential of about 1.5 V needs to be applied.

The Al-Ga-Zn chandlery anode came as a large cuboid, and small samples were cut out and turned down into 2 mm diameter cylinders and soldered onto a copper wire for electrochemical testing. In 2M NaCl scans were started at -2.2 V vs. SCE, and in 8M KOH at -2.1 V vs. SCE. The scan rate was set at 50 mV s^{-1} and a temperature of ~ 294 K was used (*Figure 3.5.4*).

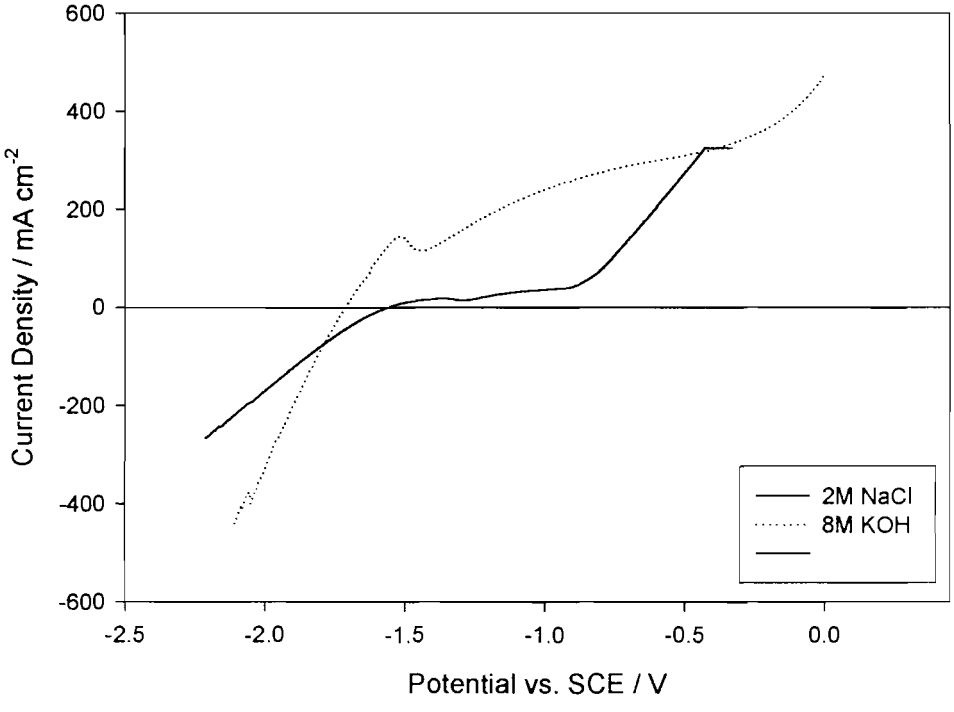

***Figure 3.5.4* – Voltammetry data obtained for Al-Zn-Ga Chandlery Anode (area ~ 0.2 cm^2) in 8M KOH and 2M NaCl solutions at a scan rate of 50 mV s^{-1}, resolution of 1 mV and a temperature of ~294 K.**

A zinc dissolution peak at ~ -1.5V, can clearly be seen in the data for 8M KOH in *Figure 3.5.4*. Considerable anodic and cathodic currents are seen in both electrolytes, with an overpotential of ~ 1V needed to produce them with 2M NaCl.

Table 3.5.5 shows the open circuit potentials for each of the alloy/electrolyte systems and compares the potentials for each at 50 and 100 mA cm^{-2}.

	2M NaCl			8M KOH		
Alloy	**OCP vs. SCE /V**	**Potential at 50 mA cm^{-2} /V**	**Potential At 100 mA cm^{-2} /V**	**OCP vs. SCE /V**	**Potential at 50 mA cm^{-2} /V**	**Potential at 100 mA cm^{-2} /V**
High Purity Aluminium	-1.8	(-)	(-)	-2.0	-1.3	-0.7
Meltspun Aluminium	-1.6	-0.4	-0.35	-1.6	-0.8	(-)
Aluminium Magnesium	-1.6	-0.6	-0.5	(*)	(*)	(*)
SAFT Anode	-1.6	-0.5	-0.4	-1.8	-1.75	-1.6
Al-Zn-Ga Anode	-1.6	-0.8	-0.7	-1.75	-1.7	-1.6
AB50V Anode	-1.7	-1.1	-1.0	-2.0	-1.9	-1.8

Table 3.5.5– Comparing the open circuit potential (OCP), and the potentials at 50 and 100 mA cm^{-2}, in 8M KOH and 2M NaCl, for each of the alloys tested.

(-) current density was not reached within the potential range of the graph.

(*) sample dissolved too rapidly on discharge to be tested.

According to *Table 3.5.5* the AB50V alloy and the SAFT anode would perform best in an Al-air battery based on KOH electrolyte. They both show high rates of corrosion on open circuit. No alloy currently tested, however, shows both stability to corrosion and significant dissolution at low overpotentials. In chloride solution, stability to corrosion is good; but even with the best alloy (AB50V), only low potentials and current densities are achieved. The chloride ions are not able to effectively pit the oxide film formed on the alloy surface unless large overpotentials are applied. Hydroxide ions in KOH solutions

complex the Al(III) formed leading to large corrosion rates on open circuit. They do, however, have good potentials/current densities on discharge. This is a commonly found result throughout the literature.

The shaded results in *Table 3.5.5* show possible systems for adding the electrolyte immediately before use. They all show reasonable potentials for 50 and 100 mA cm^{-2} current densities. Only samples in solutions of KOH show good enough potentials for use in this application. The three samples shown to be the best possible systems of those tested contain alloying elements of Zn, Sn, Mg, and Ga in small amounts. The benefits of these alloying elements are heavily discussed in the literature.

3.6 Test Battery System with High Purity Aluminium

The battery test cell was made up of two parallel electrodes (nominal area ~ 2 cm^2); one a commercial platinum catalysed air cathode, the other an aluminium electrode. The separation between the electrodes was controlled by polymer gaskets and holes in the top of the cell allowed for flowing of electrolyte if needed. The high purity aluminium was in wire format (d = 1 mm) and four strands were wrapped around a carbon block to make a contact. The total area exposed to the solution was ~ 0.3 cm^2 spread across the 2 cm^2 cathode face. Using the polymer gaskets and spacing block, tests were carried out at electrode separations of 0.3 and 1.2 cm. The anode was placed at the top of the setup to minimise leakage, and the experiment was undertaken at a temperature of ~ 294 K. The electrolyte was added immediately prior to discharge via the channel tubes located at the top of the cell. The cell was tested with both 8M KOH and 2M NaCl. Firstly, the current was varied linearly with time (10 mA cm^{-2} / min) and the battery voltage plotted, then the sample was held at 40 mA cm^{-2} for one hour and the battery voltage plotted. *Figure 3.6.1* to *Figure 3.6.3* shows these results for high purity aluminium in 8M KOH.

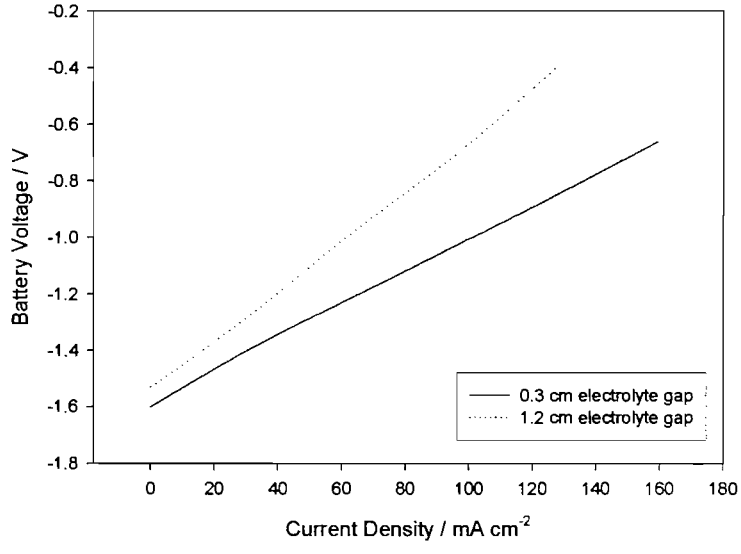

Figure 3.6.1 – Graph showing Battery Voltage /V versus Current Density /mA cm^{-2} for test battery cell in 8M KOH with 0.3 cm^2 of high purity aluminium with 0.3 and 1.2 cm electrode separation.

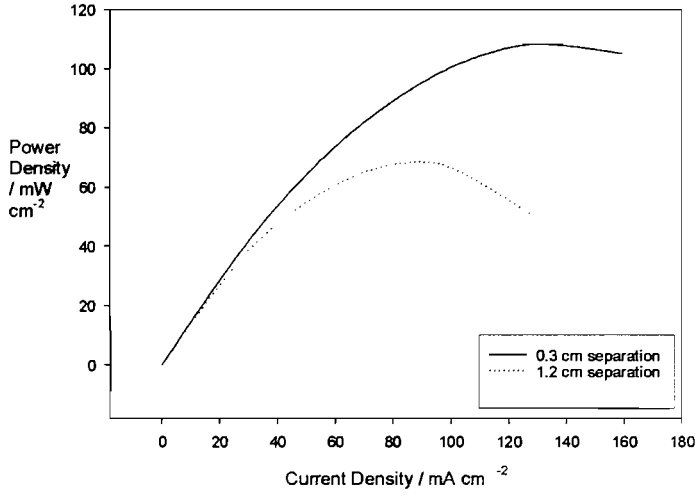

Figure 3.6.2 – Graph showing Power Density / mW cm^{-2} versus Current Density / mA cm^{-2} for test battery cell with 0.3 cm^2 of high purity aluminium in 8M KOH with 0.3 and 1.2 cm electrode separations.

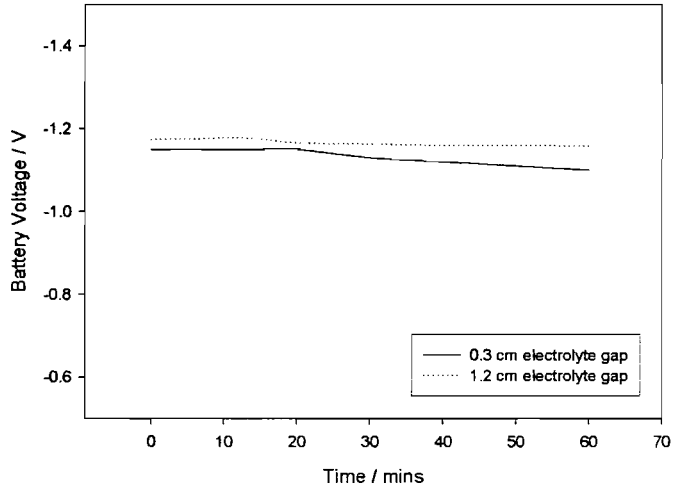

Figure 3.6.3 – Graph showing Battery Voltage /V versus Time /mins for test battery cell in 8M KOH with 0.3 cm^2 of high purity aluminium with 0.3 and 1.2 cm electrode separation. Held at 40 mA cm^{-2}.

Figure 3.6.1 shows good cell voltages, at low current densities (i.e. under 30 mA cm^{-2}), of about 1.5 V, which decreases to about 1.0 V at 100 mA cm^{-2}. Both plots are seen to be roughly linear over the current range tested and as expected the 0.3 cm separation shows more negative battery voltages for corresponding current densities. It is expected that the IR drop of the electrolyte between the electrodes in the 1.2 cm separation case, will be much greater than that of the 0.3 cm case. *Figure 3.6.2* shows that the peak power density is observed around 140 mA cm^{-2} for the 0.3 cm separation, and much lower at 90 mA cm^{-2} for the 1.2 cm separation. It is clear from *Figure 3.6.3* that at a current density of 40 mA cm^{-2}, the battery voltage can be maintained for a period of at least an hour.

The above experiments were then repeated for high purity aluminium in 2M NaCl, the results of which can be seen in *Figure 3.6.4* to *Figure 3.6.6*.

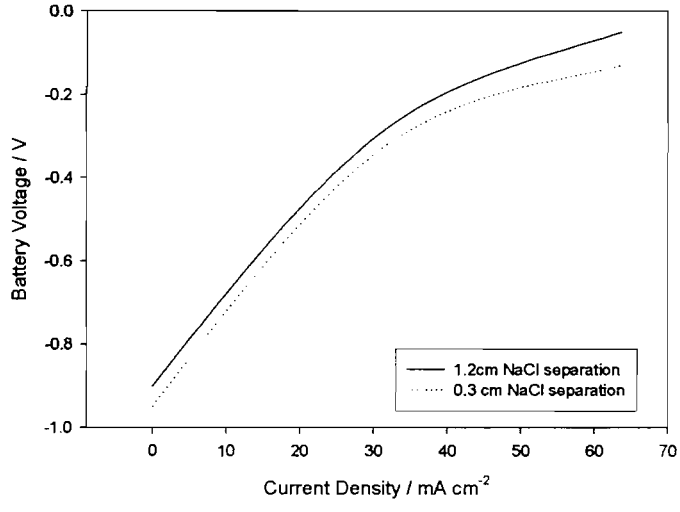

Figure 3.6.4 – Graph showing Battery Voltage /V versus Current Density /mA cm^{-2} for test battery cell in 2M NaCl with 0.3 cm^2 of high purity aluminium with 0.3 and 1.2 cm electrode separations.

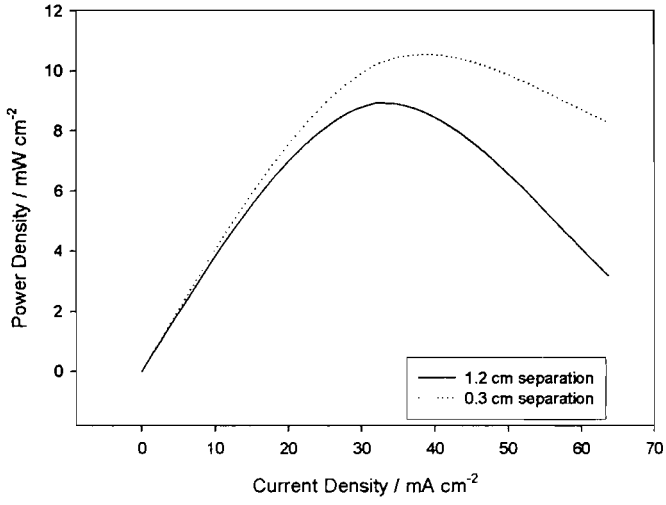

Figure 3.6.5 – Graph showing Power Density / mW cm^{-2} versus Current Density / mA cm^{-2} for test battery cell with 0.3 cm^{-2} of high purity aluminium in 8M KOH at electrode separations of 0.3 and 1.2 cm^{2}.

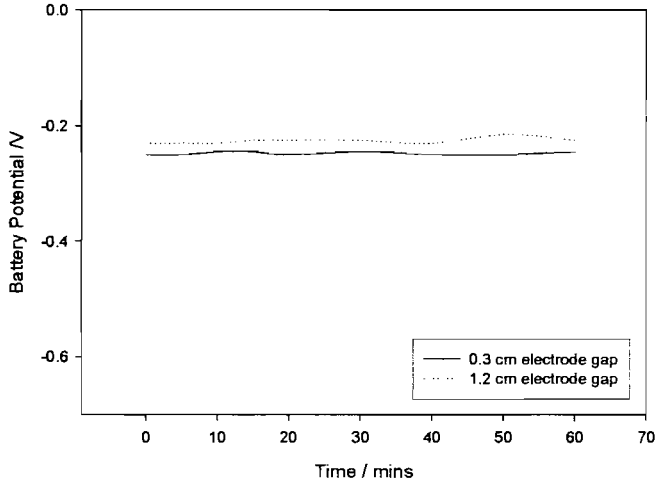

Figure 3.6.6 – Graph showing Battery Voltage /V versus Time /mins for test battery cell in 2M NaCl with 0.3 cm^{2} of high purity aluminium with 0.3 and 1.2 cm electrode separations. Held at 40 mA cm^{-2}.

In 2M NaCl a much lower cell voltage is observed over the entire current range. From *Figure 3.6.4* it can be seen that even at zero current drawn the voltage does not reach 1.0 V. Unlike with 8M KOH, a purely linear relation is not observed; at higher current densities the gradient of the line steadily decreases. Peak power densities can be taken from *Figure 3.6.5* as ~ 40 mA cm^{-2} for the 0.3 cm separation and ~ 30 mA cm^{-2} for the 1.2 cm separation. These are considerably lower than those seen in 8M KOH. *Figure 3.6.6* shows that at 40 mA cm^{-2} it is still possible to maintain a constant battery voltage over the hour timeframe but the battery voltage is very small (~ 0.2 V).

3.7 Test Battery System with AB50V

With AB50V one strip of the sheet was wrapped around the carbon block giving an area exposed to solution of 0.3 cm^2.

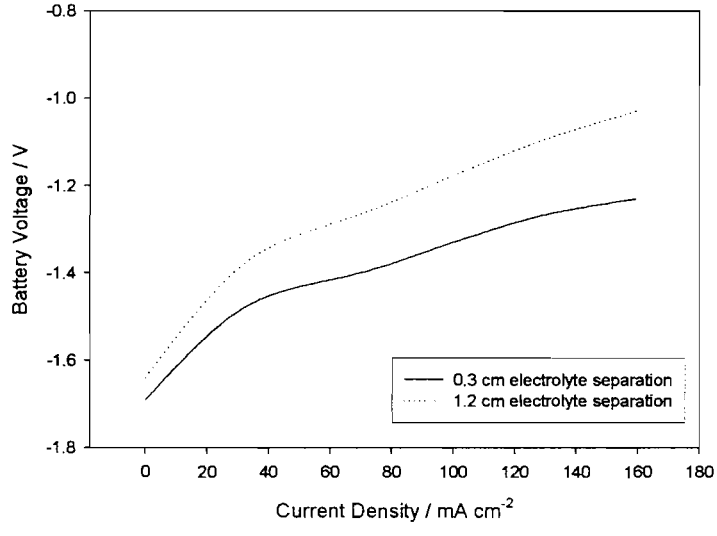

Figure 3.7.1 – Graph showing Battery Voltage /V versus Current Density /mA cm^{-2} for test battery cell in 8M KOH with 0.3 cm^2 of AB50V alloy with 0.3 and 1.2 cm electrode separations.

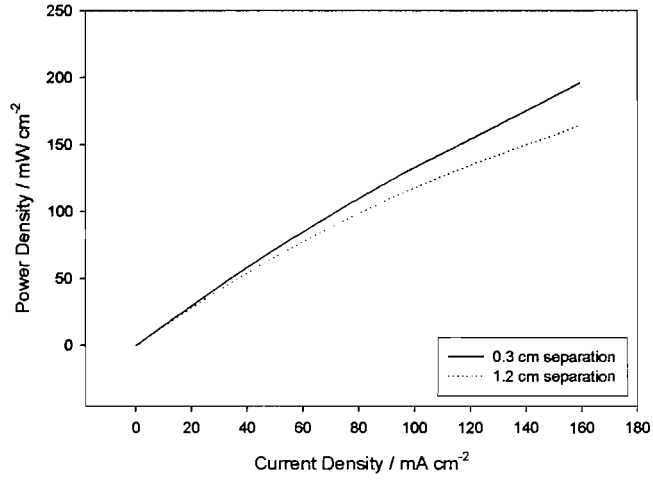

Figure 3.7.2 – Graph showing Power Density / mW cm^{-2} versus Current Density / mA cm^{-2} for test battery cell in 8M KOH with 0.3 cm^2 of AB50V alloy with 0.3 and 1.2 cm electrode separations.

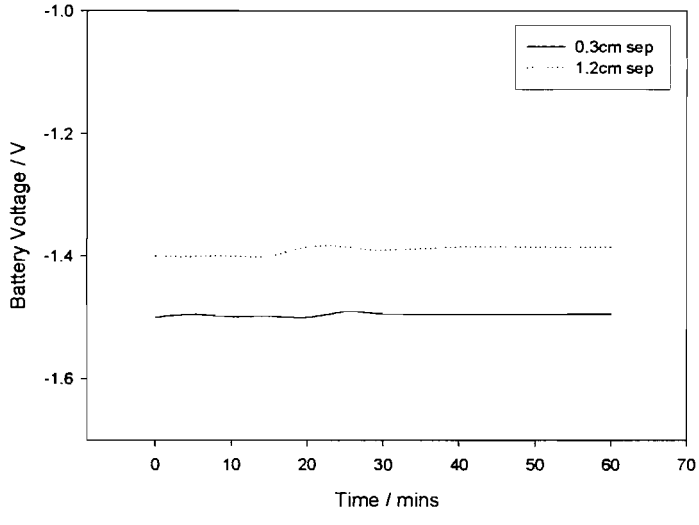

Figure 3.7.3 – Graph showing Battery Voltage /V versus Time /mins for test battery cell in 8M KOH with 0.3 cm^2 of AB50V alloy with 0.3 and 1.2 cm electrolyte gaps. Held at 40 mA cm^{-2}

Figure 3.7.1 shows good cell voltages; better than with high purity aluminium in 8M KOH for corresponding current densities. There are two clear linear regions present between 0 to 35 mA cm^{-2}, and 60 to 140 mA cm^{-2}. The power density plot (*Figure 3.7.2)* does not pass through a maximum over the current density range tested. As with the other results, *Figure 3.7.3* shows a constant battery voltage for the period of an hour when held at 40 mA cm^{-2}. The battery voltage of 1.5 V is very satisfactory. In all repeats, AB50V appears superior to high purity aluminium.

As with high purity aluminium, the AB50V was also tested in 2M NaCl. *Figure 3.74* to *Figure 3.7.6* report the results.

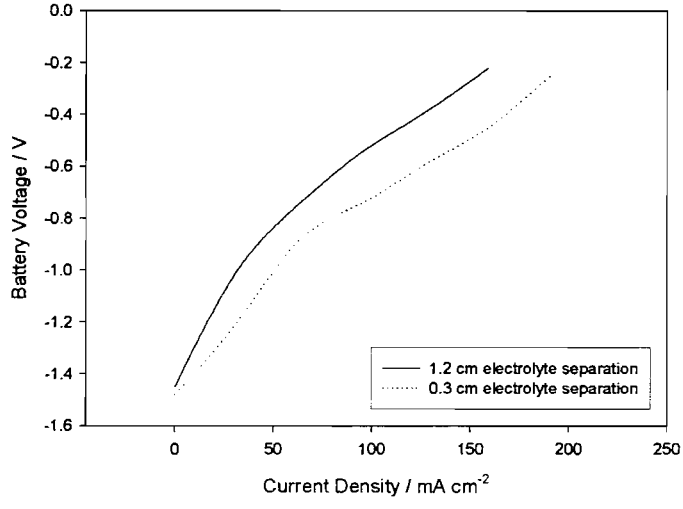

Figure 3.7.4 – Graph showing Battery Voltage /V versus Current Density /mA cm^{-2} for test battery cell in 2M NaCl with 0.3 cm^2 of AB50V alloy with 0.3 and 1.2 cm electrolyte gaps.

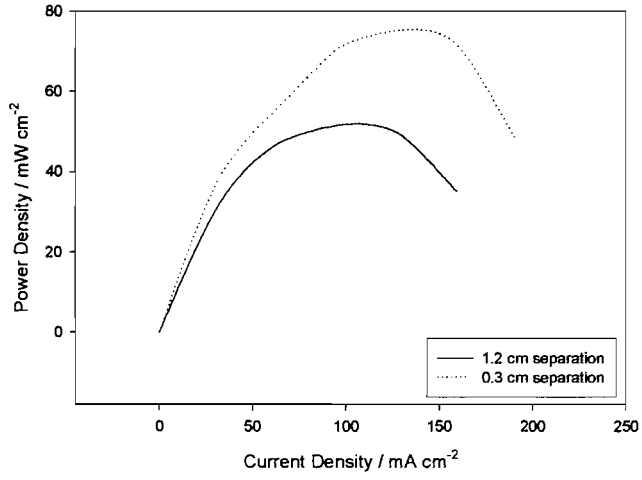

Figure 3.7.5 – Graph showing Power Density / mW cm^{-2} versus Current Density / mA cm^{-2} for test battery cell with 0.3 cm^2 of AB50V in 2M NaCl with electrode separations of 0.3 and 1.2 cm.

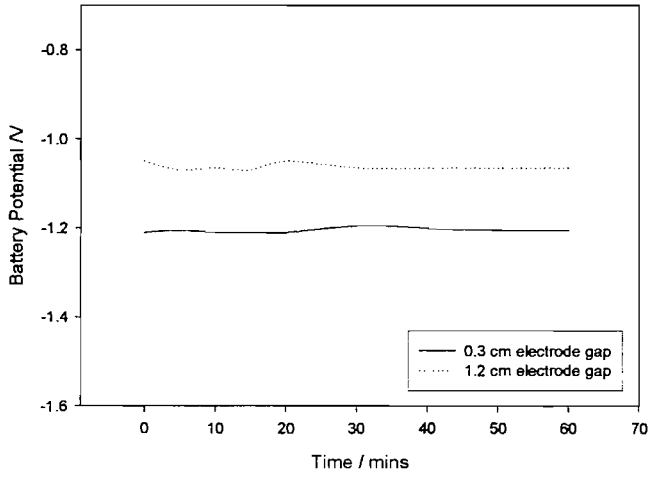

Figure 3.7.6– Graph showing Battery Voltage /V versus Time /mins for test battery cell in 2M NaCl with 0.3 cm^2 of AB50V alloy with 0.3 and 1.2 cm electrolyte gaps. Held at 40 mA cm^{-2}.

Compared with high purity aluminium in 2M NaCl, much better cell voltages are observed across the current density range in *Figure 3.7.4*. Peak power densities are shown in *Figure 3.7.5* as being around 150 mA cm^{-2} for the 0.3 cm separation and around 100 mA cm^{-2} for the 1.2 cm separation. Constant battery voltage was observed over the hour at 40 mA cm^{-2} (*See Figure 3.7.6*).

Electrode Separation / cm	High Purity Aluminium in 8M KOH		High Purity Aluminium in 2M NaCl		AB50V Alloy in 8M KOH		AB50V Alloy in 2M NaCl	
	j /mA cm^{-2}	E / V	j /mA cm^{-2}	E / V	j /mA cm^{-2}	E / V	j /mA cm^{-2}	E /V
0.3	140	-0.8	40	-0.25	>160	< -1.3	150	-0.55
1.2	90	-0.9	30	-0.3	>160	< -1.0	100	-0.5

Table 3.7.7 – Table showing the current density / mA cm^{-2} and the cell voltage / V of the test cell with the four different systems tested at both 0.3 and 1.2 cm electrode separations (Figures 3.6.1 – 3.7.6).

AB50V in 8M KOH gives very promising battery voltages of 1.3 V with current densities exceeding 150 mA cm^{-2}.

With high purity aluminium in 8M KOH showing good battery voltages at low current densities it is a possible for low current density applications. By far the best in 2M NaCl was the AB50V again showing possible battery voltage for low current density applications. It is clear from *Table 3.7.7* that AB50V out performs high purity aluminium in both electrolytes. With a good final battery voltage being around -1.5 V and a current density of > 50 mA cm^{-2}, we can see that only AB50V in 8M KOH is a suitable choice.

3.8 High Surface Area Investigations

One of the aims of the project is to investigate high surface area 3-D electrodes with structural properties such that they can comprise part of the plane's structure. An experiment was undertaken to investigate whether such a structure could be produced by compressing layers of wires/fibres in various lay-ups, and whether compression alone would be enough to give these structures the required strength. Both meltspun fibres and high purity aluminium wires were used. Stainless steel plates were used in an Ingstrom Compressor to apply pressure to the samples. Only qualitative tests of strength were achievable due to the frailty of samples and limited supply of meltspun aluminium.

Four structures of interlaced wires/fibres were used during experimentation. These can be seen in *Figure 3.8.1:* Structure A (two perpendicular layers of wires); Structure B (woven mesh); Structure C (five wires twisted together to make one and then placed in perpendicular layers); and Structure D (randomly lain wires).

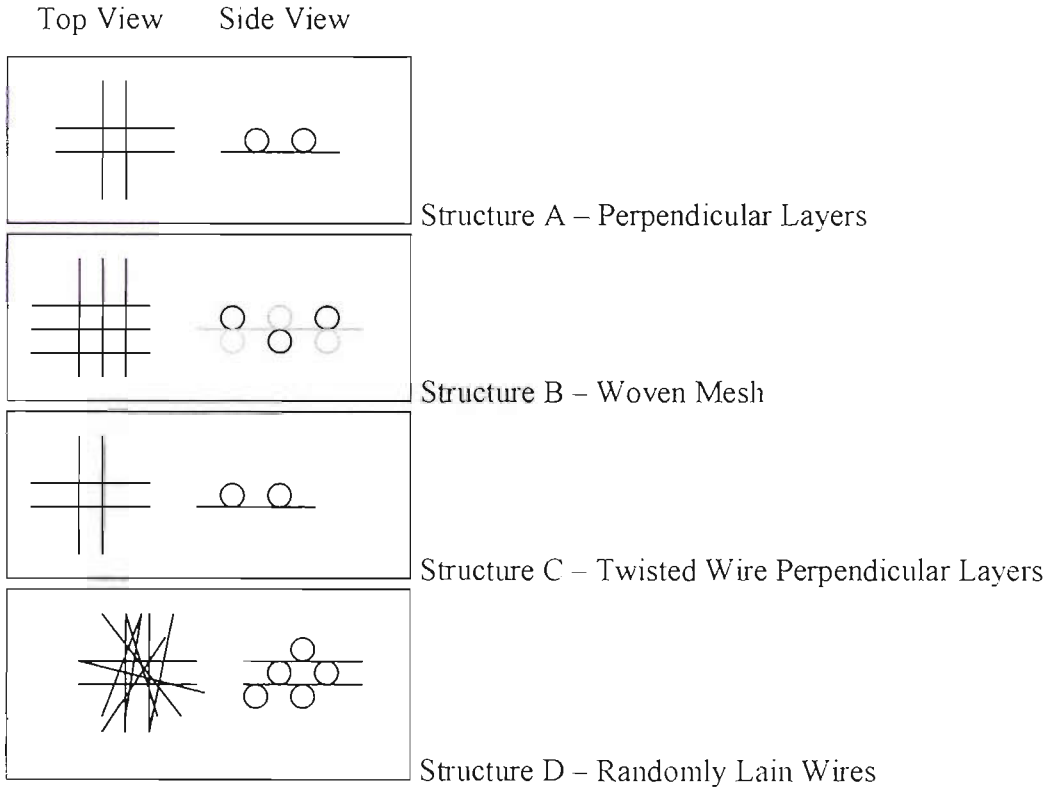

Figure 3.8.1 – The four structures employed in the compression testing of meltspun/high purity aluminium. * 5 wires twisted together to make one strand

Below are some of the SEM images of the resulting meshes/layers after compression has taken place.

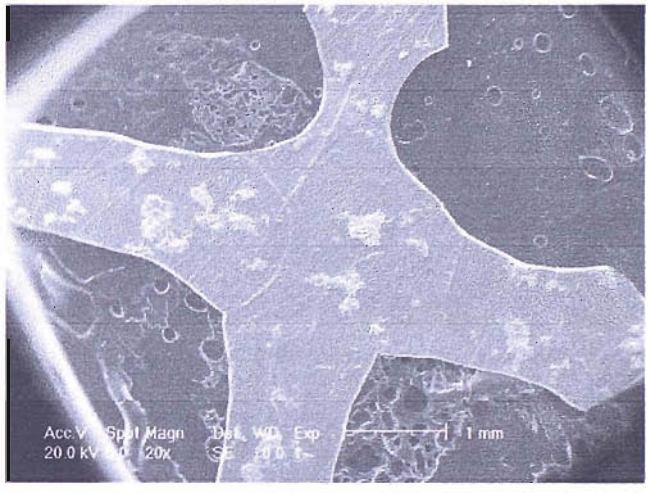

Figure 3.8.2 – High purity aluminium individual layer of structure A compressed to 100 kN

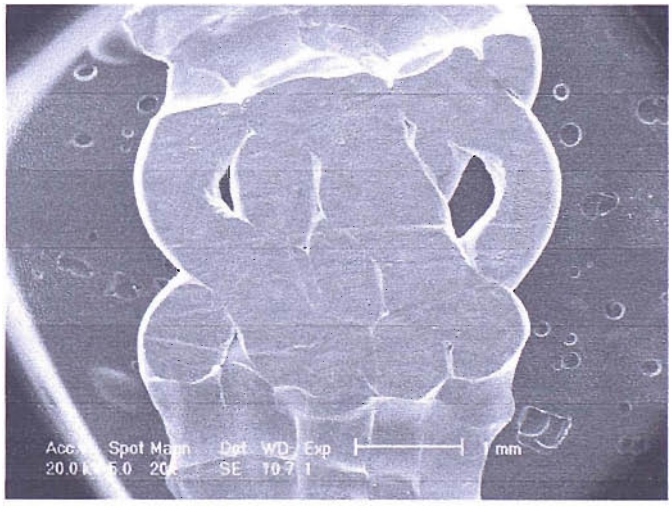

Figure 3.8.3 – High purity aluminium individual layer of structure C compressed to 50 kN

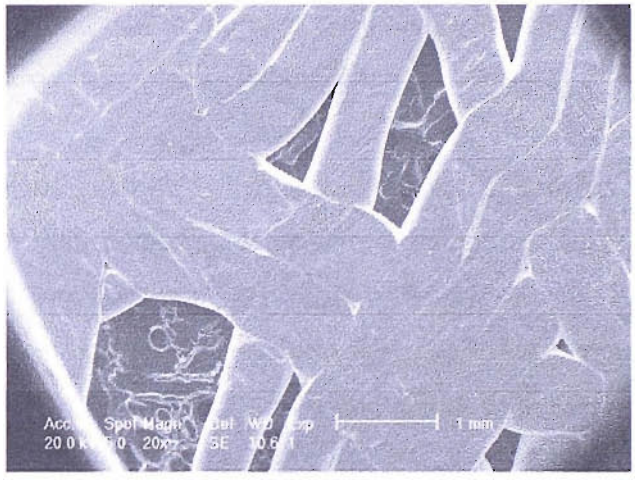

Figure 3.8.4 – High purity aluminium individual layer of structure D compressed to 100 kN

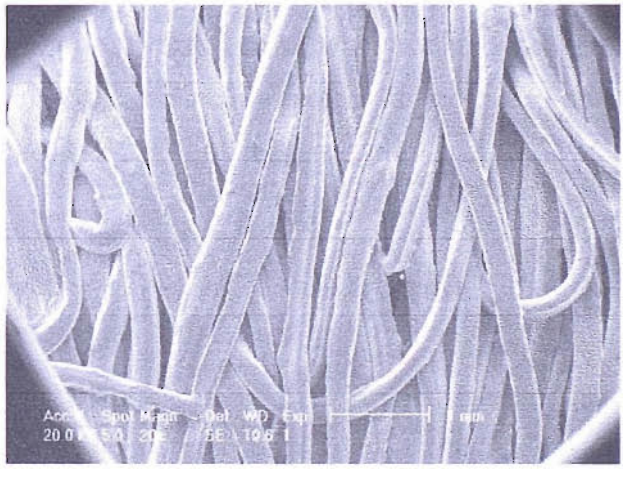

Figure 3.8.5 – Meltspun fibre mesh consisting of three layers using the structure A. These have been compressed to 100 kN.

With high purity aluminium, the only way to get good structural integrity was to compress the wires to greater than 100kN. This effectively compressed them into a plate and so a high surface area was not necessarily gained (See Figure 3.8.2). No large scale structures were made with the high purity aluminium that were able to be moved and handled without them falling apart. *Figure 3.8.3* and *Figure 3.8.4* show structure C and D respectively. Structure C showed good adhesion within the twisted strands but little or no adhesion between the twisted strands. This meant it fell apart easily on movement. Structure D, the randomly lain wires, showed relatively good adhesion but still not good enough to stay

together on movement, and due to the high compression of 100 kN having to be used to achieve this the wires were completely flattened.

The meltspun aluminium, however, when placed in four or more layers of structure D and compressed to 100kN had considerable structural strength. These compressed meshes could be handled and were even quite malleable without breakage. Figure 3.8.5 shows the top layer of one of these compressed meshes. Any cutting of the mesh attempted always led to the mesh falling apart. Due to a lack of suitability of the meltspun aluminium alloy and difficulties in production of other, more suitable, alloys via the same technique - no more production experiments were undertaken.

One commercial alloy foam was tested electrochemically. The foam (10 ppi) was cut into small sections (volume ~ 0.06cm^3) and soldered onto the end of a copper wire, for testing. The foam was Goodfellow's 6101 alloy foam.

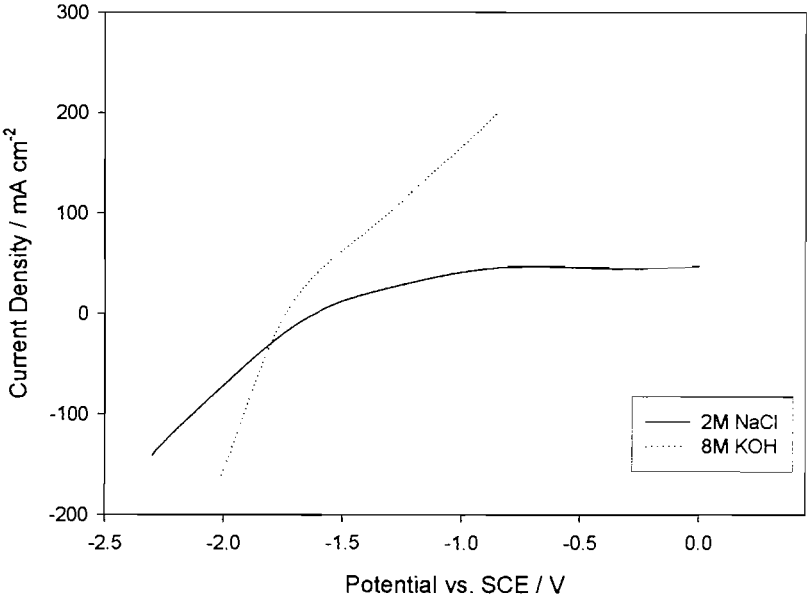

Figure 3.8.6 – Voltammetry data obtained for 6101 alloy foam (area ~0.5 cm^{-2}) in 8M KOH and 2M NaCl. Taken at scan rate of 50 mV s^{-1}, and a temperature of ~ 294 K.

A very large cathodic current can be observed in *Figure 3.8.6* for 6101 alloy foam in both 8M KOH and 2M NaCl. The open circuit potential is ~ -1.7 V in 8M KOH and ~ -1.6 V

for 2M NaCl. Considerable slopes through the open circuit potentials must be noted, showing extensive corrosion. Although the current densities are encouraging, it must be noted that the area of the sample tested is only estimated due to the complexity of measuring the surface area of the foam. This could mean large discrepancies in the current densities. Future work must be based on foams manufactured from better alloys.

4. Conclusion

There are several clear conclusions that can be drawn from the thesis. It is clear that in both KOH and NaCl media, the rates of open circuit corrosion and the current density/potential response for the anodic dissolution of the aluminium depend strongly on the purity and composition of the aluminium material. Moreover, some aluminium materials dissolve uniformly while others dissolve to give very complex surface structures. The experimental programme has been constrained by the limitation to commercially available alloys which are, in fact, very limited and often their compositions are poorly specified. As a result, it remains speculation as to the preferred alloying components and certainly it is not possible to optimize the level of alloy elements; this influences both the fundamental understanding of the behaviour and the development of a battery. The ideal of a material completely stable on open circuit and dissolving rapidly at a low overpotential has not been achieved. Therefore, a practical battery would have to be based on flooding with electrolyte immediately before discharge.

"Impure" aluminium certainly corrodes very rapidly in both saline and alkaline electrolyte. Common impurities in aluminium include iron (a good catalyst for hydrogen evolution), magnesium, and silicon, at a relatively high level. High purity aluminium faired much better and there is a real need for alloys manufactured from pure aluminium with low additions of other metals. Understanding of the properties also requires that a range of alloy compositions are available with each component varied over a narrow range so that the role of each alloying element can be defined. Good alloying elements for further investigation appear to be indium, gallium, tin, and zinc.

Based on measurements of open circuit potential, voltammetry, and SEM during dissolution, AB50V alloy, an Al-Mg-Sn-Ga alloy, has been identified as a preferred anode material in concentrated potassium hydroxide. It has an open circuit potential of ~ -2.0 V vs. SCE and dissolves with a current density of 100 mA cm^{-2} at an overpotential of just 0.2 V. It also showed the best performance of all the alloys tested in 2M NaCl. All the alloys are more stable to corrosion in brine medium. In 2M NaCl, AB50V alloy gives an open circuit potential of ~ -1.7 V vs. SCE and dissolves with a current density of around 100 mA cm^{-2} at -1.0 V vs. SCE.

The laboratory test Al/air battery with 2 cm^2 (maximum size) electrodes performed reasonably well with both the AB50V alloy and high purity aluminium as the anode. The batteries showed an almost constant voltage during discharge for one hour over a range of current densities. A typical battery voltage was ~ 1.3 V at current densities in excess of 160 mA cm^{-2} with an AB50V alloy anode and 8M KOH electrolyte. The maximum power density was in excess of 200 mW cm^{-2}. It should also be stressed that the cell was not optimized by reducing the interelectrode gap or other design parameters. The battery performance should be enhanced substantially if foams and other three-dimensional materials were available in the selected aluminium alloys.

The work in this thesis has confirmed that the weight of the electrolyte is the limiting factor in determining the battery performance in the application for small aircraft power. The weight of the electrolyte is determined by the volume required to dissolve all the Al(III) formed during battery discharge and to maintain both electrodes in an active state. Potassium hydroxide electrolyte is significantly better than NaCl solutions in this respect but the literature indicates that the solubility of Al(III) in 8M KOH is approximately 1.6 M at room temperature. It would be interesting to investigate other electrolytes in order to seek higher solubility. Of course, the electrolyte must also give the other desired properties – stability to corrosion and a high rate of anodic dissolution at low overpotentials. Possible electrolytes would be based on organic acids that are polydentate ligands for Al(III). The alternative approach would be to allow the Al(III) to deposit as the oxide but to ensure that the oxide layer has a structure that permits continued high rate dissolution.

It would be interesting to examine the influence of corrosion inhibitors on the behaviour of aluminium alloys. Would they inhibit corrosion on open circuit but still allow anodic dissolution? Perhaps cathodic inhibitors would be particularly attractive.

The application of the battery as a power source for a micro-aircraft leads to many intriguing possibilities as to the positioning and structure of the battery. The feasibility of using a high surface area three-dimensional aluminium structure has always been a possibility. Because of the low weight of the current structural polymer material used, ideas such as using the battery as the wing or tail structure have been abandoned. Current thinking is leaning towards a battery that forms a skin around the nose cone of the plane.

This has the advantages of perhaps allowing improved structural integrity of the nose cone while allowing more volume within the fuselage (where the current lithium polymer battery is sited in close proximity to the electronic instrumentation) for useful components for surveillance and monitoring. Separation of the batteries from the surveillance and monitoring equipment would also reduce the heating of the electronics due to Joule heating during battery discharge.

References

[1] L. Newcome, A Brief History of Unmanned Aviation, AIAA, 2004
[2] S. M. Ltd., http://www.airforce-technology.com/projects/predator/, 2005.
[3] B. B. S. R. Ltd, A Flight Control Design Methodology For Micro Air Vehicles, 2003,
[4] B. B. S. R. Ltd., Machine Vision in UAV Control Systems, 2004,
[5] R. Jones, G. Morris, Journal of Defence Science 5 (2000) 227-234.
[6] T. Ltd., http://www.thunderpower-batteries.com, 2005.
[7] J. Kruger, http://electrochem.cwru.edu/ed/encycl/art-c02-corrosion.htm, 2005.
[8] M. Pourbaix, Atlas of Electrochemical Equilibria in Aqueous Solution, Pergamon Press, Oxford, 1966
[9] D. Pletcher, A First Course In Electrode Processes, The Electrochemical Consultancy, 1991
[10] M. Hulot, Comptes Rendes Hebdomadaire des Seances de l'Acadamie des Sciences 40 (1855) 148.
[11] D. Tommasi, Traite des Piles Electriques (1889) 131.
[12] S. Zaromb, Journal of the Electrochemical Society 109 (1962) 1125.
[13] L. Trevethan, D. Bockstiem, S. Zaromb, Journal of the Electrochemical Society 110 (1963) 267.
[14] Q. Li, N. J. Bjerrum, Journal of Power Sources 110 (2002) 1-10.
[15] W. H. Hoge, Low Cost Gas Diffusion Electrodes for Electrosynthesis, International Forum on Electrolysis in the Chemical Industry, Lake Buena Vista, Florida, USA, 1993.
[16] M. W. Dodson, Aluminium Alloys for Battery Anodes in Alkaline Systems, in, Chemistry, vol University of Southampton, Southampton, 1992, p.^pp. 164.
[17] A. Dobley, J. Robak, Final Report on Research of Air Cathodes for Aluminium-Air Batteries, 2004,
[18] E. D. Linden, Aluminum/Air Batteries, in: Handbook Of Batteries, vol McGraw Hill, 1994, p.^pp. 38.22-38.39.
[19] C. D. S. Tuck, Modern batteries, Ellis Horwood Limited, 1991
[20] S. H. Yang, H. Knickle, Journal of Power Sources 112 (2002) 162-173.
[21] Shao Hua Yang, H. Knickle, Journal of Power Sources 124 (2003) 572-585.
[22] Xin Zhang, Shao Hua Yang, H. Knickle, Journal of Power Sources 128 (2004) 331-342.
[23] J. P. Iudice de Souza, W. Vielstich, Seawater aluminium/air cells, in: Handbook of Fuel Cells - Fundamentals, Technology & Applications, vol 1, John Wiley & Sons, 2003, p.^pp.
[24] N. A. Popovich, R. Govind, Journal of Power Sources 112 (2002) 36-40.
[25] W. A. Ferrando, Journal of Power Sources 130 (2004) 309-314.
[26] Z. Z. Lazarevic, V. B. Miskovic-Stankovic, Z. Kacarevic-Popvic, D. M. Drazic, Corrosion Science 47 (2005) 823-834.
[27] P. Campestrini, G. Goeminne, H. Terryn, J. Vereecken, J. H. W. d. Wit, Journal of the Electrochemical Society 151 (2004) 59-70.
[28] J.-K. Chang, C.-M. Lin, C.-M. Liao, C.-H. Chen, W.-T. Tsai, Journal of the Electrochemical Society 151 (2004) 188-194.

[29] P. Y. Deng, X. D. Bai, X. W. Chen, Q. L. Feng, Journal of the Electrochemical Society 151 (2004) 284-289.
[30] K.C. Emregul, A. A. Aksut, Corrosion Science 42 (2000) 2051-2067.
[31] M.L. Doche, J.J. Rameau, R. Durand, F. Novel-Cattin, Corrosion Science 41 (1999) 805-826.
[32] P. Carbonini, T. Monetta, D.B. Mitton, F. Bellucci, P. Mastronardi, B. Scatteia, Journal of Applied Electrochemistry 27 (1997) 1135-1142.
[33] M. Paramasivam, M.Jayachandran, S. V. Iyer, Journal of Applied Electrochemistry 33 (2003) 303-309.
[34] M. Paramasivam, S. V. Iyer, Journal of Applied Electrochemistry 31 (2001) 115-119.
[35] K.-K. Lee, K.-B. Kim, Corrosion Science 43 (2001) 561-575.
[36] I. John Albert, M. Anbu Kulandainathan, M.Ganesan, V.Kapali, Journal of Applied Electrochemistry 19 (1989) 547-551.
[37] H.B. Shao, J.M. Wang, Z. Zhang, C. N. Cao, Materials Chemistry and Physics 77 (2002) 305-309.
[38] H.A. El Shayeb, F.M. Abd El Wahab, S. Z. E. Abedin, Journal of Applied Electrochemistry 29 (1999) 473-480.
[39] C.D.S. Tuck, J.A. Hunter, G. M. Scamans, Journal of the Electrochemical Society 134 (1987) 2970-2981.
[40] A. M. M. M. Adam, N. Borras, E. Perez, P. L. Cabot, Journal of Power Sources 58 (1996) 197-203.
[41] S. Z. E. Abedin, A. O. Saleh, Journal of Applied Electrochemistry 34 (2004) 331-335.
[42] S. Z. E. Abedin, F. Endres, Journal of Applied Electrochemistry 34 (2004) 1071-1080.
[43] A.J. Bard, R. Parsons, J. Jordan, Standard Potentials in Aqueous Solution, Marcel Dekker Inc., 1985
[44] A.G. Munoz, S.B. Saidman, J. B. Bessone, Corrosion Science 44 (2002) 2171-2182.
[45] A.G. Munoz, J. B. Bessone, Corrosion Science 41 (1999) 1447-1463.
[46] A.A. Mazhar, S.T. Arab, E. A. Noor, Journal of Applied Electrochemistry 31 (2001) 1131-1140.
[47] E. Van Gheem, J. Vereecken, C. L. Pen, Journal of Applied Electrochemistry 32 (2002) 1193-1200.
[48] H. Sato., 205th Meeting of the Electrochemical Society, Inc. (2004) Abs. 123.
[49] J. Kawakita, K. Kobayashi, Journal of Power Sources 90 (2000) 182-187.
[50] H.B. Shao, J.M. Wang, X.Y. Wang, J.Q. Zhang, C. N. Cao, Electrochemistry Communications 6 (2004) 6-9.
[51] P. Suresh, A.K. Shukla, S.A. Shivashankar, N. Munichandraiah, Journal of Power Sources 110 (2002) 11-18.
[52] M.L. Doche, F. Novel-Cattin, R. Durand, J. J. Rameau, Journal of Power Sources 65 (1997) 197-205.
[53] D.M. Drazic, J. P. Popic, Journal of Applied Electrochemistry 29 (1999) 43-50.
[54] R. Huang, K. R. Herbert, T. Gessmann, K. G. Lynn, Journal of the Electrochemical Society 151 (2004) 227-232.
[55] Q. Meng, G. S. Frankel, Journal of the Electrochemical Society 151 (2004) 271-283.
[56] C. E. D. D. Macdonald, Journal of Applied Electrochemistry 20 (1991) 405.
[57] D.D. Macdonald, S. Real, M. Urquidi-Macdonald, Journal of the Electrochemical Society 135 (1988) 2397-2409.

[58] D.D. Macdonald, S. Real, S. I. Smedley, M. Urquidi-Macdonald, Journal of the Electrochemical Society 135 (1998) 2410-2414.
[59] D.D. Macdonald, C. English, Journal of Applied Electrochemistry 20 (1990) 405-417.
[60] S. Real, M. Urquidi-Macdonald, D. D. Macdonald, Journal of the Electrochemical Society 135 (1988) 1633-1636.
[61] D. R. Salinas, S. G. Garcia, J. B. Bessone, Journal of Applied Electrochemistry 29 (1999) 1063-1071.
[62] H. A. E. Shayeb, F. M. A. E. Wahab, S. Z. E. Abedin, Journal of Applied Electrochemistry 29 (1999) 473-480.
[63] S.A. Salih, A.G. Gad-Allah, A.A. Mazhar, R. H. Tammam, Journal of Applied Electrochemistry 31 (2001) 1103-1108.
[64] Y. Tang, L. Lu, H. W. Roesky, L. Wang, B. Huang, Journal of Power Sources (2004).
[65] E. Brillas, P. L. Cabot, F. Centellas, J. A. Garrido, E. Perez, R. M. Rodriguez, Electrochimica Acta 43 (1998) 799-812.
[66] M. A. Hernandez, Corrosion (2002) 1-11.
[67] J. W. Schultze, M. M. Lohrengel, Electrochimica Acta 45 (2000) 2499-2513.
[68] A. E. Simone, L. J. Gibson, Acta Materia 46 (1998) 3109-3123.
[69] C. C. Yang, H. Nakae, Journal of Alloys and Compounds 313 (2000) 188-191.
[70] J. F. Rakow, A. M. Waas, Mechanics of Materials 37 (2005) 69-82.
[71] J. Zhou, Z. Gao, A. M. Cuitino, W. O. Soboyejo, Materials Science and Engineering 111 (2004) 189-194.
[72] Y. Feng, H. Zheng, Z. Zhu, F. Zu, Materials Chemistry and Physics 78 (2002) 196-201.
[73] I. Duarte, J. Banhart, Acta Materia 48 (2000) 2349-2362.
[74] J. A. Curran, Novel Open-Celled Aluminium Foams For Air Batteries: Production and Mechanical Properties, 2002,
[75] J. Zhou, P. Shrotriya, W. O. Soboyejo, Mechanics of Materials 36 (2004) 781-797.
[76] A. M. Harte, N. A. Fleck, M. F. Ashby, Acta Materia 47 (1999) 2511-2524.
[77] K. Y. G. McCullough, N. A. Fleck, M. F. Ashby, Acta Materia 47 (1999) 2331-2343.
[78] E. Davis, ASM Speciality Handbook: Aluminium and Aluminium Alloys, ASM International, 1993